



## ORIGINAL ARTICLE

# Adsorption of cadmium(II) in wastewater by magnesium oxide modified biochar



Yingjie Xu, Hongying Xia \*, Qi Zhang, Guiyu Jiang, Wuchen Cai, Wenhai Hu

Faculty of Metallurgy and Energy Engineering, Kunming University of Science and Technology, Kunming 650093, Yunnan, China  
State Key Laboratory of Complex Nonferrous Metal Resources Clean Utilization, Kunming University of Science and Technology, Kunming 650093, Yunnan, China

Yunnan Provincial Key Laboratory of Intensification Metallurgy, Kunming University of Science and Technology, Kunming 650093, Yunnan, China

Key Laboratory of Unconventional Metallurgy, Ministry of Education, Kunming 650093, Yunnan, China

Received 16 March 2022; accepted 15 June 2022

Available online 20 June 2022

## KEYWORDS

*C. oleifera* shells;  
Regeneration;  
Thermodynamics;  
Kinetics

**Abstract** A new MgO-AC (magnesium oxide modified activated carbon) adsorbent was successfully synthesized under microwave irradiation. XRD, FT-IR, XPS, SEM and N<sub>2</sub> adsorption were used to characterize the properties of MgO-AC. It was found that MgO-AC was highly crystalline under the preparation process, and the doping of MgO (Magnesium oxide) did not cause the gap blockage of AC (activated carbon), but the micropore area and average pore size of modified AC increased significantly. Multiple conditional parameters were studied to determine the optimal adsorption effect, such as roasting temperature, holding time, MgO doping amount, contact time, adsorption temperature, system pH, and initial concentration of Cd(II) (divalent cadmium ion). The results show that the optimal parameter conditions are as follows: the insulation temperature is 800 °C, holding time of 40 min, the doping amount of MgO is 1/20 of AC, and the maximum adsorption capacity is 649.9 mg·g<sup>-1</sup> at pH = 7. In addition, thermodynamic studies show that the adsorption process is spontaneous and endothermic, and kinetic and adsorption isotherm models show that the pseudo-second-order kinetic model and Langmuir model are well fitted for the adsorption process.

© 2022 The Author(s). Published by Elsevier B.V. on behalf of King Saud University. This is an open access article under the CC BY-NC-ND license (<http://creativecommons.org/licenses/by-nc-nd/4.0/>).

\* Corresponding author at: State Key Laboratory of Complex Nonferrous Metal Resources Clean Utilization, Kunming University of Science and Technology, Kunming, Yunnan 650093, China.

E-mail address: [hyxiakust@163.com](mailto:hyxiakust@163.com) (H. Xia).

Peer review under responsibility of King Saud University.



Production and hosting by Elsevier

## 1. Introduction

Water is the source of life; all human activities are closely related to water. However, in recent years, China, the United States, Japan and other countries have reported that some marine, river, wetland or freshwater resources are being polluted by a large number of heavy metals (Wattigney et al., 2019; Soto-Ramirez et al., 2021; Verma and Dwivedi, 2013; Akinci et al., 2013; Duan et al., 2020) These heavy metals are mainly derived from wastewater-discharged from electroplating industry, mining, metallurgy industry, battery manufacturing,

petroleum refining, tannery, paint manufacturing, pesticide, pigment manufacturing and printing industry (Park et al., 2017; Li et al., 2017). Cd is an excellent metal for neutron absorption and a byproduct of zinc smelting process. It is dispersed in some water bodies through welding, electroplating, cadmium-nickel battery, nuclear fission plant, paint, plastic and chemical fertilizer (Burakov et al., 2018; Tian et al., 2019). The World Health Organization stipulates that the maximum concentration of Cd(II) in drinking water should be less than  $0.003 \text{ mg}\cdot\text{L}^{-1}$  (WHO, 2011). In addition, the presence of Cd(II) in wastewater can be very harmful pollutant as a heavy metal and can easily accumulate in organisms. Although Cd(II) has no pathological significance, its compounds are highly toxic. If it is discharged directly without treatment, it is easy to cause chronic poisoning of human beings and animals. Long-term exposure to low concentrations of Cd(II) compounds will cause anemia, emphysema, neuralgia, stomach pain, osteoporosis and other emergencies (Liu et al., 2022; Fu et al., 2021). Therefore, the effective treatment of wastewater containing Cd(II) is urgent, the removal of Cd(II) from wastewater environmental significance for researchers to develop efficient, green treatment technologies.

So far, various physical and chemical methods have been used to remove heavy metal ions from wastewater. These include chemical precipitation, electrolysis, ion exchange and microbial methods (Jian et al., 2018; Da'na, 2017; Tao et al., 2015). Although these methods can effectively remove some heavy metal ions in wastewater, they are often costly. At the same time, a large number of toxic sludge and by-products will also be produced in the removal process, causing secondary pollution to the environment (Gupta et al., 2021; Li et al., 2018). Among them, adsorption method is the process of separating adsorbate from solution and gathering adsorbate on adsorbent by Van der Waals force. This process has the characteristics of non-toxic, economic and environmental protection, and renewable use, so it is considered to be able to effectively remove heavy metals from wastewater by replacing other processes (Liu et al., 2020; Asere et al., 2019; Xu et al., 2021a,b; Xu et al., 2022). In recent years, a large number of adsorbents have been used to study the removal of heavy metals in wastewater. For example, Belova (Belova, 2019) uses natural zeolite in Yagodnisky deposit to adsorb nickel, copper, and other heavy metals in solution. The adsorption material has high cation exchange capacity, strong corrosion resistance and wide application range. The maximum adsorption capacity of metal ions is  $0.023 \text{ mg}\cdot\text{eq}\cdot\text{g}^{-1}$ . Zhu (Zhu et al., 2022a,b) reported a new type of adsorption material with layered cationic skeleton containing phosphonium salts, which was used to remove  $\text{Fe}^{3+}$  and  $\text{Zn}^{2+}$  in drinking water. The material contained C-PO(OH)<sub>2</sub> group, which would have a strong chelating effect with metal ions. Finally, the maximum adsorption capacities of  $\text{Fe}^{3+}$  and  $\text{Zn}^{2+}$  were  $206.03 \text{ mg}\cdot\text{g}^{-1}$  and  $281.36 \text{ mg}\cdot\text{g}^{-1}$ , respectively. Otunola (Otunola and Olofade, 2020) reported the study on the effective adsorption of heavy metals in water by some clay minerals. The adsorption characteristics of this kind of adsorbent were attributed to the large specific surface area and the presence of unsaturated charges on the surface, which would adsorb some anions and cations in the liquid. Duan (Duan et al., 2022) used 6-acryloylamino-N-hydroxyhexanamide resin to adsorb heavy metal ions. The resin showed high adsorption performance for  $\text{Cu}^{2+}$  and  $\text{Pb}^{2+}$ , which was mainly attributed to the fact that the CONHOH group on its surface would produce a stable five-membered ring matrix with heavy metal ions, to achieve the purpose of removing metal ions. Zhu (Zhu et al., 2021) removed heavy metal ions in water by phosphate modified anionic clay. The maximum adsorption capacities of  $\text{Cr}^{3+}$  and  $\text{Cd}^{2+}$  reached  $156.95 \text{ mg}\cdot\text{g}^{-1}$  and  $198.34 \text{ mg}\cdot\text{g}^{-1}$ , respectively. Yan (Yan et al., 2022) removed the divalent heavy metals in water by Facile bleaching of ethylene tetramethylene phosphonic acid into UiO-66. This material has large adsorption capacity and excellent stability, and is considered as a new adsorbent. However, the above adsorbents still have some defects in the adsorption process, such as small adsorption capacity, poor thermal and chemical stability, low adsorption rate, poor recyclable performance, high process cost or difficult preparation

(Jun et al., 2019). Therefore, it is necessary to find an ideal adsorbent with large specific surface, high adsorption capacity, renewable and high selectivity. Activated carbon is a very popular adsorption material, which is widely used in industrial water treatment because of its large specific surface area and pore size, low price, and recyclable characteristics (Hashem et al., 2021). But often pure activated carbon has less adsorption sites and less functional groups, which is very unfavorable for the adsorption of different substances. Domestic and foreign scholars have done a lot of modification work on activated carbon, such as adding metal oxides (Foroutan et al., 2022), metal salts (Igwegbe et al., 2021), organic compounds (Elashry et al., 2022; Yang et al., 2021), alkaline earth metals (Przepiórski et al., 2013) and transition metals (Hakim et al., 2015). Recently, it has been reported that magnesium oxide has weak hydrolysis in water, which can generate free hydroxyl groups and these hydroxyl functional groups will selectively adsorb pollutants in water. Under the action of electrostatic adsorption, hydroxyl with negative charge will adsorb heavy metal ions with positive charge. However, with the decrease of MgO particle size, the increased surface can inevitably lead to poor stability. Due to van der Waals force or other interactions, particles with smaller diameter are more likely to aggregate, which leads to the decrease or even loss of MgO adsorption performance with smaller diameter. It has been reported that loading MgO on activated carbon with large specific surface area can increase the active adsorption site of AC (Cheng et al., 2018), and avoid the decrease of adsorption capacity caused by MgO agglomeration in water. Therefore, some scholars fixed magnesium salt directly on AC by sol-gel method (Ghalekhondabi et al., 2021; Vu et al., 2016) and evaporation-induced self-assembly method (Zhou et al., 2018; Ghaemi et al., 2021), and mixed it to obtain MgO-AC adsorption material by tube furnace roasting.

*C. oleifera* is a unique woody edible oil tree species in China, which is widely distributed in various provinces of southern China. Usually in the production and processing, in order to increase the oil yield of *C. oleifera* and reduce the wear of equipment, the shell will be removed preferentially, which will lead to a large amount of *C. oleifera* shells called agricultural wastes (Li et al., 2016). However, *C. oleifera* shells contains more cellulose, hemicellulose, lignin, a certain number of polyphenols and a small amount of oil representing the ideal raw material for the preparation of AC. Therefore, how to make full use of *C. oleifera* shell to convert it into high value-added products and realize experimental intensive production is one of the focuses of *C. oleifera* industry research.

In this study, a new production process was proposed. Compared with the above two MgO-AC production processes, the activation of uncarburized biomass with nitric acid will destroy some chemical bonds in it, increase the porosity, increase the types of functional groups, and form a charged active site (Gokce and Aktas, 2014; Feng et al., 2020). At the same time, the activated shell of *Camellia oleifera* promoted the uniform adhesion of magnesium nitrate to pores and surfaces, and increased the active site of AC. Finally, under the action of microwave roasting, subcritical water will degrade more unactivated cellulose, hemicellulose, and lignin in biomass, producing many functional groups, which is more conducive to the removal of heavy metal ions. Therefore, in this study,  $\text{Cd}(\text{NO}_3)_2$  solution was used to simulate wastewater containing cadmium. The effects of microwave roasting temperature, holding time, solution pH, solution temperature, initial cadmium ion concentration and adsorption time on the adsorption performance of MgO-AC were studied. The adsorption process was evaluated by adsorption kinetics and thermodynamics.

## 2. Experimental

### 2.1. Material

*C. oleifera* shells used in the experiment was provided by Jiangxi Qingshui Yao Ecological Agriculture Development

Co., Ltd., magnesium nitrate ( $\text{Mg}(\text{NO}_3)_2$ , AR.) (Shanghai McLin Biochemical Technology Co., Ltd.), nitric acid ( $\text{HNO}_3$ , 2.5 M) (Shanghai McLin Biochemical Technology Co., Ltd.), sodium hydroxide ( $\text{NaOH}$ , AR.) (Shanghai McLin Biochemical Technology Co., Ltd.), cadmium nitrate ( $\text{Cd}(\text{NO}_3)_2$ , AR.) (Tianjin Zhiyuan Chemical Reagent Co., Ltd.). The whole experiment was carried out with deionized water.

## 2.2. Preparation method of MgO-AC

Firstly, deionized water was used to clean the shell debris of *C. oleifera* shells in order to remove the impurities on the surface of the material, and then it was dried at 90 °C for 4 h to constant weight. 9 g pretreated *C. oleifera* shells were put in the beaker, and then 200 mL  $\text{HNO}_3$  (nitric acid) solution (2.5 M) were added to make the lignin and cellulose hemicellulose in *C. oleifera* shells fully reacted with  $\text{HNO}_3$ . The fully reacted material was filtered and washed, and then 200 mL of  $\text{Mg}(\text{NO}_3)_2$  solution with the concentration of  $0.1 \text{ mol}\cdot\text{L}^{-1}$  ( $0.4 \text{ mol}\cdot\text{L}^{-1}$ ) were added. After being fully mixed, it was filtered, washed and dried for further use. A certain amount of the above dried materials was weighed and put into a microwave oven for roasting activation. With  $\text{N}_2$  as the protective gas, the heating temperature was 500–900 °C and the holding time was 20–40 min, a new composite material of MgO-AC was obtained. Then under the same adsorption time, MgO-AC materials obtained under different holding temperature and holding time were used to adsorb the same concentration of  $\text{Cd}(\text{II})$ . By comparing the removal rate of  $\text{Cd}(\text{II})$  by each adsorption material, the roasting temperature and holding time were selected as the optimal process to produce MgO-AC. As shown in Fig. 1.

## 2.3. Sample characterization

PW1825 X-ray diffractometer (XRD) produced by from Philips is used to reveal the crystal structure and chemical composition of the material, in which  $\text{Cu-K}\alpha$  is used as X-ray source,  $\lambda = 0.15416 \text{ nm}$ , voltage  $\leq 40 \text{ KV}$ , current  $\leq 40 \text{ mA}$ . The specific surface area, pore size distribution, and total pore volume of the material were calculated by using Autosorb-1-C nitrogen adsorption and desorption instrument to test the nitrogen adsorption capacity of the material. Field emission scanning electron microscopy (FE-SEM) (JEOL JSM-7800F) was used to observe the morphology of samples. X-ray photoelectron spectroscopy (XPS) (Thermo Fisher Scientific, ESCALAB 250Xi) was used for spectral measurement. X-ray was used as the excitation source, and monochromatic Al target X-ray source and double anode Al/Mg target X-ray source were used. The chemical information about the sample surface and interface at 1–10 nm was provided, and C1s (284.6 eV) was used as a reference. Use Fourier transform infrared spectrometer (MB3600-CH20) to detect the type of functional group of the product.

## 2.4. Adsorption study

The batch adsorption experiments were carried out in 200 mL  $\text{Cd}(\text{NO}_3)_2$  solution to study the influence of key parameters on the adsorption effect, such as pH, initial concentration of  $\text{Cd}(\text{II})$  and contact time. The final concentration of  $\text{Cd}(\text{II})$  was determined by atomic absorption spectrophotometer. The equilibrium adsorption capacity of  $\text{Cd}(\text{II})$  in MgO-AC was obtained by the following equation under equilibrium conditions (Wang et al., 2022):

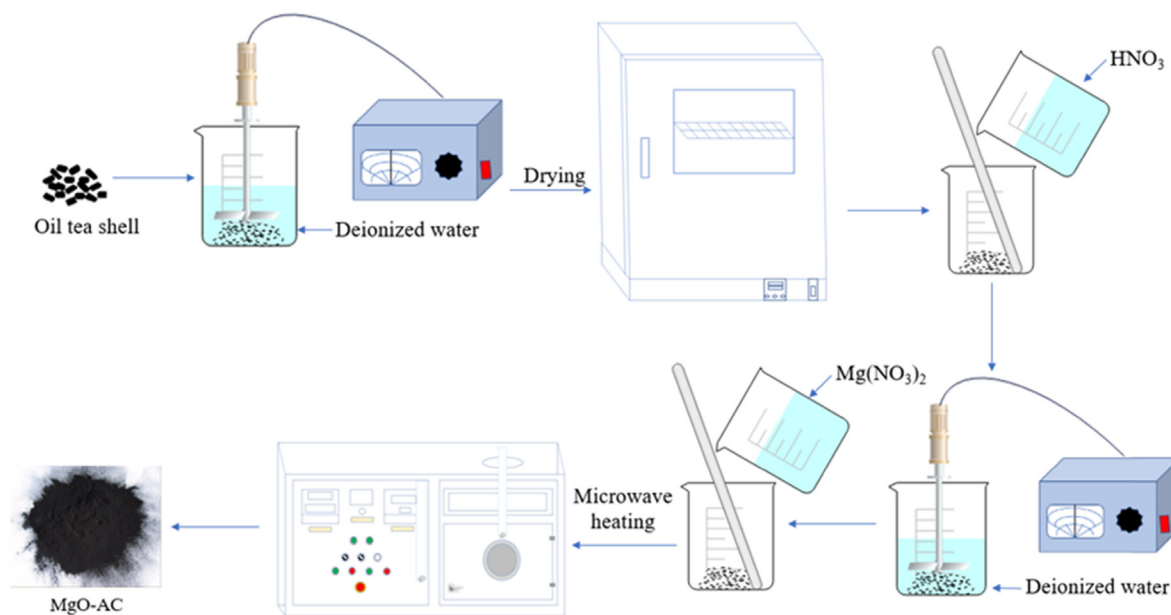


Fig. 1 Production process of MgO-AC adsorbent.

$$q_e = \frac{(C_0 - C_e)V}{M} \quad (1)$$

Among them,  $q_e(\text{mg}\cdot\text{g}^{-1})$  is equilibrium adsorption capacity,  $C_0(\text{mg}\cdot\text{L}^{-1})$  is initial concentration,  $C_e(\text{mg}\cdot\text{L}^{-1})$  is equilibrium concentration,  $V(\text{L})$  is liquid volume,  $M(\text{g})$  is adsorbent mass.

### 3. Results and discussions

#### 3.1. XRD analysis

XRD was used to reveal the phase composition and crystal structure of MgO-AC materials, as shown in Fig. 2. The samples at 24° and 44° showed obvious carbon broad peaks (Xu et al., 2021a,b; Ghaemi et al., 2022), which were attributed to (002) and (100) planes, indicating that the *C. oleifera* shells has been carbonized and has low crystallinity after microwave roasting activation. Compared with the XRD diffraction peak of AC, the crystal structure of MgO-AC changed partially. The new characteristic peaks at the diffraction angles of 43°, 62° and 78° were attributed to the diffraction peaks of MgO (Ghaemi et al., 2022; Ding et al., 2020; Borgohain et al., 2020; Yang et al., 2020), which belonged to the planes of (200), (220) and (222), indicating that MgO had been successfully doped on AC. At the same time, it can be seen from the graph that MgO-AC materials prepared by this method have better crystallinity and fewer impurity peaks. In addition, it is found that the plane (100) almost disappears after doping MgO, and the diffraction peak intensity of plane (002) also has a weakening trend, which means that the addition of MgO reduces the crystallinity of AC, tends to amorphous carbon, and has larger surface area and porosity. After the adsorption of Cd(II) by MgO-AC, the C peak disappeared, and the peak intensity of MgO weakened. At the same time, some new substances appeared. Among them, 23.7°, 30.5°, 36°, 50° and 75.2° were attributed to CdCO<sub>3</sub>, and the corresponding planes were (012), (104), (110), (116) and (128), respectively. 19.3°, 27.1°, 32.5°, 18.3°, 53.9° were attributed to the diffraction peaks of CdMg(CO<sub>3</sub>)<sub>2</sub>, a complex of Mg and Cd. The emergence of new substances may be one of the

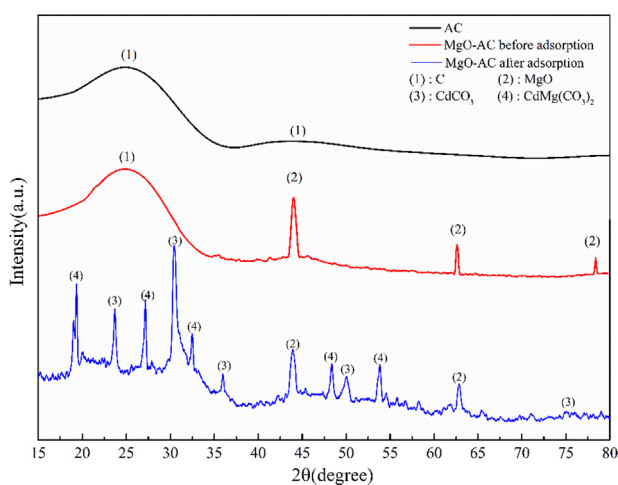


Fig. 2 XRD patterns of AC, MgO-AC before and after adsorption.

reasons for the larger adsorption capacity of MgO-AC, which may be that some functional group on MgO-AC plays an important role.

#### 3.2. BET analysis

Nitrogen adsorption measurement was carried out on MgO-AC under the optimal conditions, and BET adsorption isotherm was used to calculate the specific surface area of the measured results.

At the same temperature, the adsorption capacity of the adsorbent is often closely related to the pressure. Therefore, IUPAC (Sing, 1985; Muttakin et al., 2018) defines six adsorption isotherms according to different adsorption conditions, which are used to determine which type of adsorption the adsorption material belongs to, as shown in Fig. 3. From nitrogen adsorption - desorption curves shown in Fig. 4, it can be seen that treated AC and MgO-AC have obvious hysteresis loops. According to the six adsorption isotherms shown in Fig. 3, the adsorption curves of the adsorbent conformed to the fourth type. The flat bad points in the low relative pressure region represent the formation of monolayer dispersion, the small slope in the middle region represents the formation of multilayer dispersion. The hysteresis loop represents the capillary condensation in the mesoporous or macroporous, and the hysteresis loop is closed near the position of relative pressure  $p/p_0 = 0.4$ , indicating that the sample has a narrow mesoporous (Guo et al., 2019).

Table 1 shows the pore structure parameters of treated AC, MgO-AC and SAC. Compared with SAC, the  $S_{\text{BET}}$  of MgO-AC increases from  $29.12 \text{ m}^2\cdot\text{g}^{-1}$  to  $830.125 \text{ m}^2\cdot\text{g}^{-1}$ . The larger specific surface area makes the adsorption material have a wider contact surface with Cd(II), which will effectively increase the adsorption efficiency (Liu et al., 2018). In addition, the increase of micropore area and average pore size is

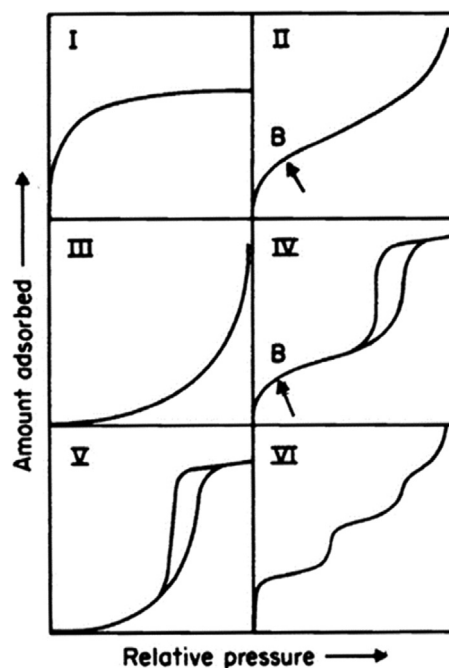


Fig. 3 Diagram of adsorption isotherm (Sing, 1985).

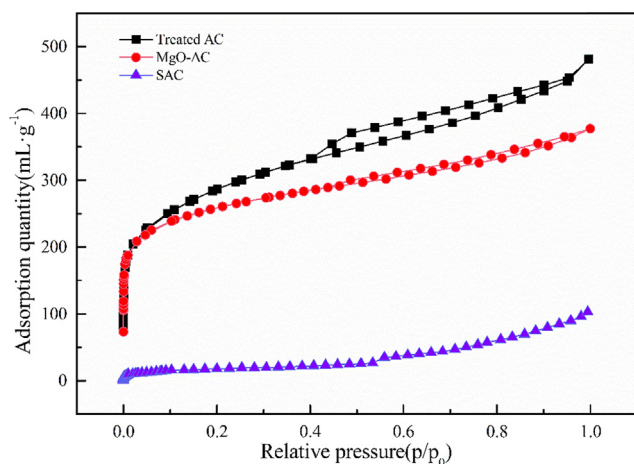


Fig. 4 N<sub>2</sub> adsorption and desorption curves.

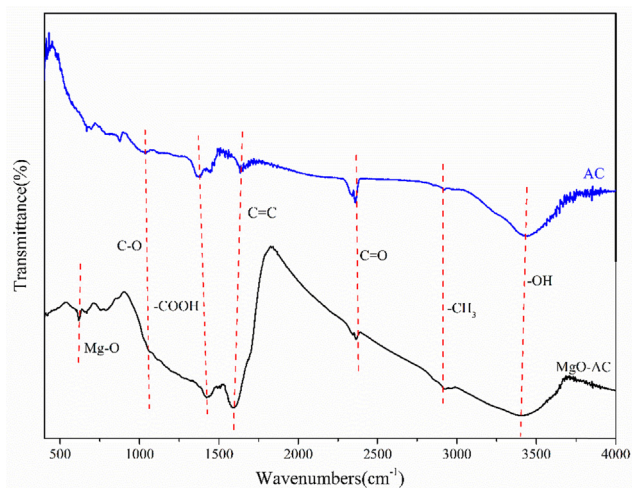


Fig. 5 FT-IR spectra of AC and MgO-AC.

Table 1 Structure parameters of aperture.

| Type of adsorbent                                   | Treated AC | MgO-AC  | SAC    |
|---|------------|---------|--------|
| S <sub>BET</sub> (m <sup>2</sup> ·g <sup>-1</sup> ) | 919.441    | 830.125 | 29.120 |
| Micropore area(m <sup>2</sup> ·g <sup>-1</sup> )    | 691.890    | 634.143 | 0      |
| Total pore volume(mL·g <sup>-1</sup> )              | 0.585      | 0.461   | 0.0316 |
| Micropore volume(mL·g <sup>-1</sup> )               | 0.277      | 0.233   | 0      |
| Average pore size(nm)                               | 1.297      | 1.069   | 0      |

beneficial to the adsorption of Cd(II), indicating that MgO-AC has an obvious effect. Compared with treated AC, the pore size parameters of MgO-AC are reduced, which is due to the penetration of MgO particles in the AC pores, so that the parameters are reduced. It was found from the decrease of each parameter that the MgO doping did not block the AC pores and the pore volume was greatly reduced, because MgO was uniformly distributed in the AC pores and no agglomeration occurred. Therefore, the synthesis of MgO-AC was considered to be very successful.

### 3.3. FT-IR analysis

FT-IR spectroscopy was used to study the functional groups of AC and MgO-AC, as shown in Fig. 5. There were several obvious peaks at 610, 1040, 1420, 1596, 2363, 2925 and 3400 cm<sup>-1</sup>, and the corresponding functional groups were Mg—O (Zhang et al., 2014), C—O (Shahrokhi-Shahraki et al., 2021), —COOH (Ghalekhondabi et al., 2021), C=C (Saleh, 2016; Haidari et al., 2016), C=O (Wang et al., 2014; Kumar et al., 2019), —CH<sub>3</sub> (Zhang et al., 2016) and —OH (Miao and Li, 2021). In addition, it was found that the peak value of MgO-AC was significantly increased compared with that of AC, indicating that the number of functional groups was significantly increased, indicating that the adsorption material had an effective oxidation effect on the adsorbent. Therefore, it can be considered that the adsorption material also had good adsorption effect on other substances. In addition, it was also found that the position of —COOH group shifted, which may be due to the position change caused by MgO doping.

### 3.4. XPS analysis

Fig. 6 shows the XPS spectra of the material. Fig. 6(a) is the broad scanning spectrum of MgO-AC before adsorbing Cd(II). At 50.08 eV, 284.08 eV and 532.08 eV, the corresponding elements are Mg2p, C1s, O1s. Fig. 6(b) shows a new peak at 411.08 eV, which is attributed to Cd3d. It shows that the adsorbent can effectively adsorb Cd(II). Fig. 6(c) shows the change of Mg binding energy before and after MgO-AC adsorption, and it is found that the binding energy of Mg increases by 0.93 eV after adsorption, which may be due to the change of Mg—O bond after adsorption of Cd(II). New chemical bonds or Cd(II)-containing complexes are produced in the adsorbent material, which changes the potential between the electronic sites and leads to the increase of the binding energy of Mg2p (Ming et al., 2016). Fig. 6(d) shows that the binding energy of Cd(NO<sub>3</sub>)<sub>2</sub> after adsorption decreases from 404.9 eV and 411.8 eV to 403.7 eV and 410.8 eV, respectively, indicating that after Cd(II) is adsorbed, it has a special effect with MgO-AC, which increases the electron cloud density around Cd. Similar phenomena are also found in Yoo (Yoo et al., 2020) and Anggraini (Anggraini et al., 2019). At the same time, according to the standard binding energy, it was found that the binding energy of Cd—O bond was consistent with that of Cd(II) adsorbed. However, no obvious oxidation process occurred in the adsorption process, which made Cd oxidized to CdO. Fig. 6(e) is the O1s spectrum before Cd(II) adsorption by MgO-AC. The peaks at 530.2 eV, 531.2 eV, 532.0 eV and 533.0 eV are attributed to MgO, O=C, —COOH and O—C, respectively (Ayiania et al., 2020; Khajuria et al., 2020; Chen et al., 2004). Fig. 6(f) is the O1s spectrum after Cd(II) adsorption by MgO-AC. Two new characteristic peaks at 529.8 eV and 530.2 eV are found, which are considered to be CdCO<sub>3</sub> and CdMg(CO<sub>3</sub>)<sub>2</sub> (Caballero-Briones et al., 2015). In addition, the binding energy of MgO and CdCO<sub>3</sub> after adsorption is also found to shift. Therefore, these phenomena prove that after adsorption, new chemical bonds or Cd-containing complexes are indeed formed in the adsorbent, which is consistent with the results shown in Fig. 2.

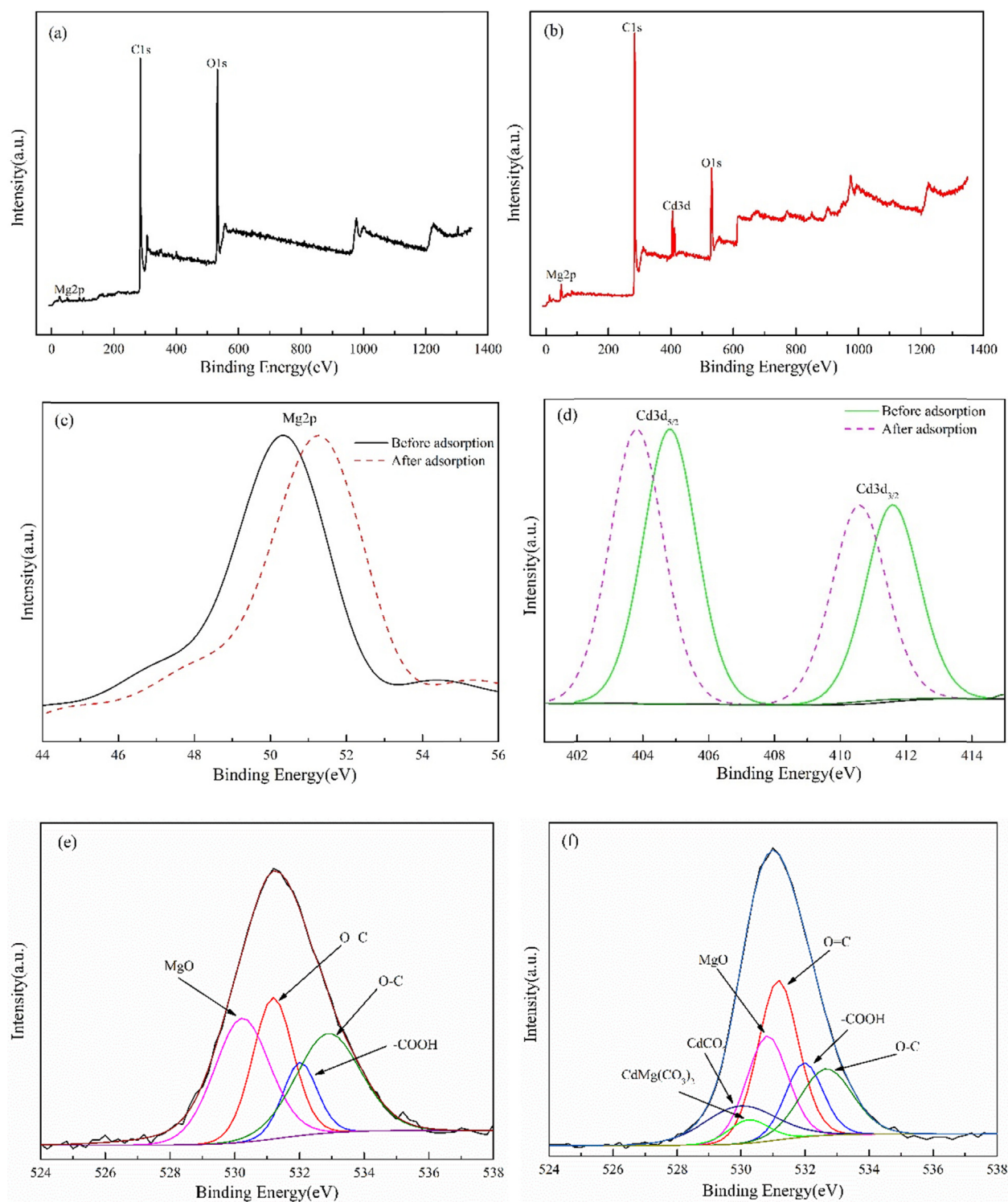


**Fig. 6** Wide scanning spectrum before MgO-AC adsorption (a); Wide scanning spectrum after adsorption of MgO-AC (b); Mg2p spectra (c); Cd3d spectra (d); O1s before adsorption(e); O1s after adsorption(f).

### 3.5. SEM-EDS analysis

**Fig. 7(a)** Biomass carbon prepared from *C. oleifera* shells by microwave calcination at 800 °C. The biochar without HNO<sub>3</sub> soaking and MgO modification has many surface

impurities and small pore size, which is very unfavorable to the adsorption process. **Fig. 7(b)** shows the images of activated biochar. At this time, the pores of the adsorption material are clear and the pore structure is rich. The doped MgO particles are uniformly distributed in the AC pores, and the particles are

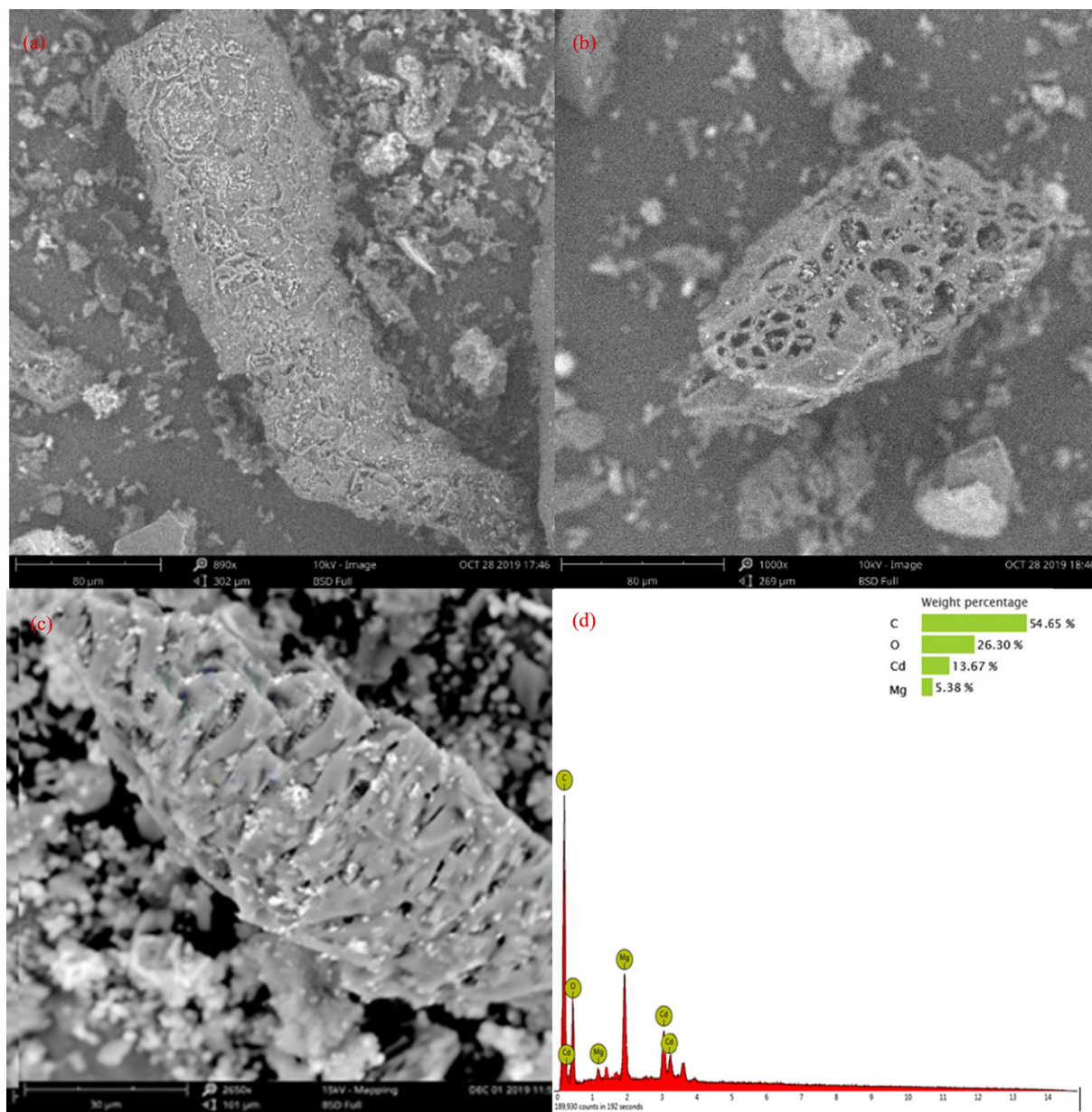


**Fig. 7** Biochar obtained only by calcination (a); before Cd(II) adsorption by MgO-AC (b); after adsorption (c); EDS image after adsorption (d).

small, without agglomeration. This is mainly due to the special doping method, which avoids the accumulation of MgO flocculation and prevents AC pore blockage, which is very beneficial to the adsorption of Cd(II). Fig. 7(c) shows the images of MgO-AC adsorbed Cd(II), and it can be seen that there are a large number of white substances on the surface of AC. This is due to the electrostatic adsorption of magnesium oxide and the adsorption of Cd(II) by intra-sphere complexation, complex  $\text{CdMg}(\text{CO}_3)_2$  of Mg and Cd was produced. Fig. 7(d) shows the EDS scanning images after Cd(II) adsorption in Fig. 7 (c). It can be seen from the mass percentage of elements that a large number of Cd(II) are adsorbed in  $\text{Cd}(\text{NO}_3)_2$  solution. At this time, the mass fractions of C, O, Cd and Mg in the material are respectively 54.65%, 26.3%, 13.67%, and 5.38%. It indicated that Cd(II) had been largely adsorbed,

and MgO-AC composites showed excellent adsorption properties.

### 3.6. Adsorption experiment

A cadmium nitrate solution with known concentration was prepared to simulate the adsorption of Cd(II) in wastewater. The effects of initial Cd(II) concentration and pH of the solution system on the adsorption of MgO-AC were studied by single variable method. The experiment was carried out in batch.

#### 3.6.1. Effect of Cd(II) concentration on adsorption performance

In order to detect the adsorption capacity of MgO-AC at different initial concentrations of Cd(II), 20 mg MgO-AC was added to several conical flasks containing 200 mL  $\text{Cd}(\text{NO}_3)_2$

solution. The concentration of Cd(II) was 25–150 mg·L<sup>-1</sup>, the pH value of the solution was 7, and the adsorption time was 200 min. The pH of the solution was adjusted by HNO<sub>3</sub> (2.5 M) and NaOH (sodium hydroxide, 1.0 M). Fig. 8 shows that when the initial concentration is 25 mg·L<sup>-1</sup>, the removal rate of Cd(II) by MgO-AC is more than 95%, and the removal efficiency decreases with the increase of the concentration of Cd(II) in the solution. When the concentration of Cd(II) in the solution was 50 mg·L<sup>-1</sup>, the adsorption rate of MgO-AC was about 92%. When Cd(II) concentration increased to 150 mg·L<sup>-1</sup>, the adsorption rate of MgO-AC was about 42%. In addition, it was found that with the increase of Cd(II) concentration, the adsorption tended to reach equilibrium within 100 min, which was attributed to the fact that in low-concentration Cd(II) wastewater, the active site of MgO-AC exceeded the number of Cd(II) available for adsorption, resulting in low adsorption efficiency. When the concentration of Cd(II) increases, the active sites used for adsorption are insufficient, resulting in an earlier adsorption equilibrium (Ahmadi and Esmaeili, 2018).

### 3.6.2. Effect of pH on the adsorption performance of MgO-AC

pH will affect the force between charged particles, and it is necessary to study pH factors (Alqadami et al., 2017; Naushad et al., 2016). 20 mg MgO-AC was added to several Cd(NO<sub>3</sub>)<sub>2</sub> solution containing 200 mL, the concentration of Cd(II) was 100 mg·L<sup>-1</sup>, the pH value of the solution was 2–9, the adsorption time was 120 min, the pH of the solution was adjusted HNO<sub>3</sub> and NaOH, the results were shown in Fig. 9. It can be seen from Fig. 9 that the adsorption effect of MgO-AC on Cd(II) increases with the transition of pH from acid to neutral, and the maximum adsorption rate is 65.1% at pH = 7. This is because H<sup>+</sup> and H<sub>3</sub>O<sup>+</sup> are abundant in acid system. When the adsorption process occurs, H<sup>+</sup> and H<sub>3</sub>O<sup>+</sup> will compete with Cd(II) for adsorption. At this time, H<sup>+</sup> and H<sub>3</sub>O<sup>+</sup> occupy the main adsorption sites. The adsorption material is highly protonated, so that the adsorbent has positive charge, thereby reducing the adsorption capacity of positive charge ions and increasing the electrostatic repulsion, so that the smaller the pH is, the lower the adsorption

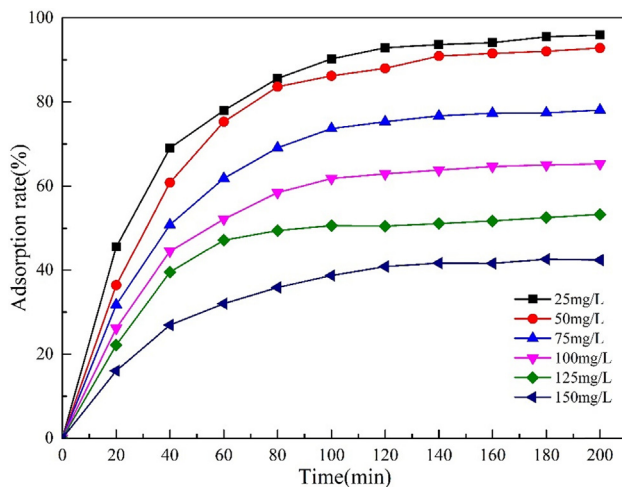


Fig. 8 Effects of different Cd(II) concentrations on the adsorption properties of MgO-AC.

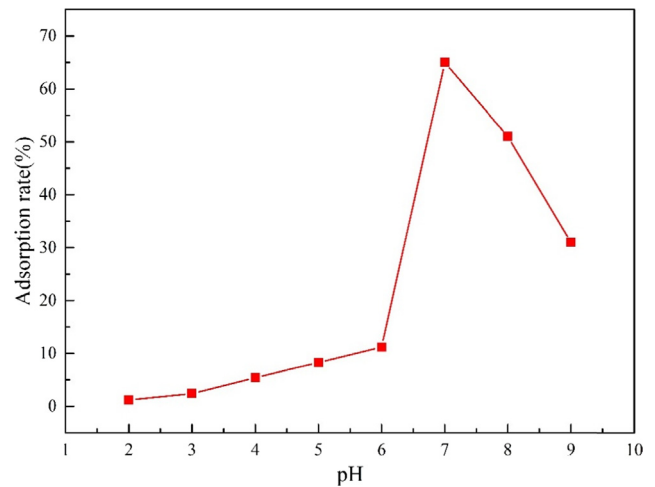


Fig. 9 Effect of pH on Cd(II) removal by MgO-AC.

efficiency is (Esmaeili et al., 2021; Naushad et al., 2019; Pushpa et al., 2015). When the pH increased to neutral, the amount of H<sup>+</sup> and H<sub>3</sub>O<sup>+</sup> in the system decreased, and the occupation ability of the adsorption sites gradually weakened, showing that the occupation ability of Cd(II) to the adsorption sites increased, so the adsorption efficiency increased. In addition, it was observed that when the pH value exceeded 7, the adsorption rate would decrease again, because under alkaline conditions, there was a large amount of OH<sup>-</sup> in the system. The Cd(II) group with positive charge would attract the OH<sup>-</sup> with negative charge, so that Cd(II) was wrapped, forming hydroxide flocs, blocking the AC gap, and reducing the adsorption rate (Goswami and Phukan, 2017). This is consistent with previous reports (Gao et al., 2019; Salamat et al., 2019).

### 3.6.3. Thermodynamics

The system temperature often has a significant impact on the adsorption performance of the adsorbent. In this work, 20 mg MgO-AC was added into a conical flask containing 100 mg·L<sup>-1</sup> Cd(NO<sub>3</sub>)<sub>2</sub> solution with a volume of 200 mL. The temperature of the system was controlled to 293 K, 303 K, 313 K and 323 K, respectively, and the system was continuously oscillating. Fig. 10 shows the effect of temperature on the adsorption performance of MgO-AC. The results showed that the removal rate of Cd(II) increased with increasing temperature. In order to determine the feasibility of the adsorption process in the heating or cooling process, K<sub>D</sub>, ΔG (kJ·mol<sup>-1</sup>), ΔS (J·mol<sup>-1</sup>·K<sup>-1</sup>), ΔH (kJ·mol<sup>-1</sup>) are calculated according to the following equation (Lima et al., 2019; Singh et al., 2018; Botelho et al., 2020):

$$K_D = \frac{(1000 * K_L * \text{molecular weight of adsorbate}) * [\text{adsorbate}]^o}{\gamma} \quad (2)$$

$$\Delta G = -RT \ln K_D \quad (3)$$

$$\Delta G = \Delta H - T\Delta S \quad (4)$$

$$\ln K_D = \frac{\Delta S}{R} - \frac{\Delta H}{RT} \quad (5)$$

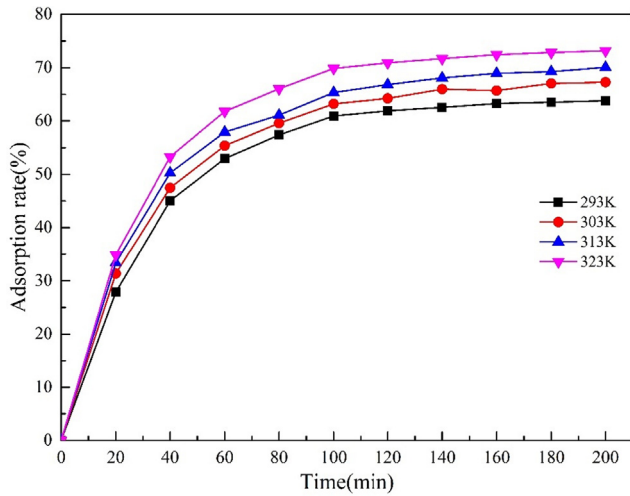


**Fig. 10** Effect of temperature on Cd(II) removal by MgO-AC.

where  $\gamma$  is the coefficient of activity (dimensionless),  $[\text{Adsorbate}]^0$  is the standard concentration of the adsorbate ( $1 \text{ mol}\cdot\text{L}^{-1}$ ).  $R$  ( $8.314 \text{ J}\cdot(\text{mol}\cdot\text{K})^{-1}$ ) is the molar gas constant,  $T$  (K) is the absolute temperature, and  $K_D$  is the thermodynamic equilibrium constant. The change value of  $\Delta G$  is calculated by Equation (4), and the values of  $\Delta H$  and  $\Delta S$  can be calculated according to the slope and intercept of  $\ln K_D$  and  $1/T$  linear fitting, as shown in Fig. 11. The regression equation is obtained after linear fitting:

$$\ln K_D = 14.8297 - 1.08043/T (r = 0.97888) \quad (6)$$

$\Delta H$  and  $\Delta S$  are calculated by equations (5) and (6), and the parameters are listed in Table 2.  $\Delta G$  is negative, and  $\Delta H$  is positive, indicating that the process of Cd(II) adsorption on MgO-AC is spontaneous and endothermic, which is consistent with the results reported in the literature (Luo et al., 2014). In the temperature range of 293–323 K, the value of  $\Delta G$  decreased from  $-27.1804 \text{ kJ}\cdot\text{mol}^{-1}$  to  $-30.8619 \text{ kJ}\cdot\text{mol}^{-1}$ , indicating that the increase of adsorption temperature promoted the adsorption of Cd(II) on MgO-AC (Guo et al., 2020; Esmaeili et al., 2021; Dakroury et al., 2020; Khan et al., 2022). The more pos-

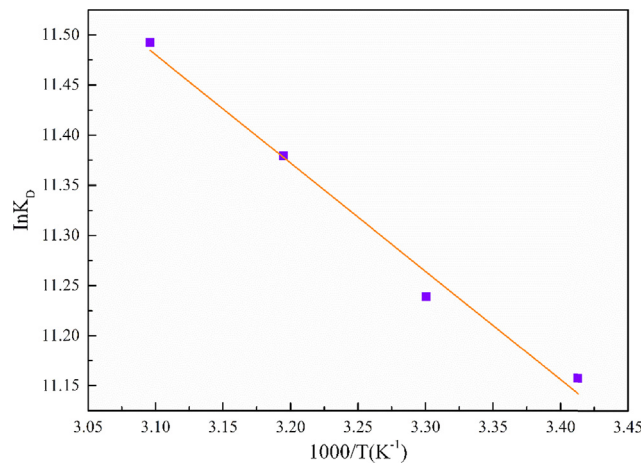


**Fig. 11** Effect of temperature on thermodynamic equilibrium constant.

**Table 2** Thermodynamic data of Cd(II) adsorption onto MgO-AC.

| T(K)  | $\ln K_D$ | $\Delta G$<br>( $\text{kJ}\cdot\text{mol}^{-1}$ ) | $\Delta H$<br>( $\text{kJ}\cdot\text{mol}^{-1}$ ) | $\Delta S$<br>( $\text{J}\cdot\text{mol}^{-1}\cdot\text{K}^{-1}$ ) |
|-------|-----------|---|---|--|
| 293 K | 11.15779  | -27.1804  | 8.9827  | 123.2941   |
| 303 K | 11.23889  | -28.3124  |   |  |
| 313 K | 11.37963  | -29.6130  |   |  |
| 323 K | 11.49237  | -30.8619  |   |  |

itive the  $\Delta H$  and  $\Delta S$  are, the greater the influence of temperature on the adsorption performance is, indicating that during the adsorption process, the temperature increases, the chaos of the system increases, and the collision probability between Cd(II) and the adsorbent at the solid-liquid interface increases, thereby improving the adsorption efficiency, which is consistent with the results shown in Fig. 10 (Hua et al., 2010; Wang et al., 2007).

#### 3.6.4. Isothermal line research

Adsorption equilibrium of Cd(II) on MgO-AC was studied. In order to explore the maximum adsorption capacity of adsorption materials for Cd(II), a certain amount of MgO-AC adsorption material was added into 200 mL, 25–150  $\text{mg}\cdot\text{L}^{-1}$  cadmium nitrate solution in several 500 mL conical flasks. Then the conical flask containing the solution was placed in a constant temperature oscillator. After constant temperature oscillation for a certain time, the supernatant was taken and filtered with a 0.22  $\mu\text{m}$  filter plug. The concentration of Cd(II) in the residual solution was determined on an atomic absorption spectrophotometer. Langmuir and Freundlich adsorption isotherm models were used to determine the nature of the adsorption process. The linear form of Langmuir isotherm equation is:

$$\frac{C_e}{q_e} = \frac{1}{q_{\max} K_L} + \frac{1}{q_{\max}} C_e \quad (7)$$

$K_L$  ( $\text{L}\cdot\text{mg}^{-1}$ ) is the Langmuir equilibrium constant, and  $q_{\max}$  ( $\text{mg}\cdot\text{g}^{-1}$ ) is the monolayer adsorption capacity (Al-Ghouthi et al., 2020b). Both are determined by the diagram of  $C_e/q_e$  and  $C_e$ . Langmuir isotherm is often evaluated by separation factor  $R_L$  (Al-Ghouthi et al., 2020a).

The Freundlich isotherm is purely empirical (Aslani and Amik, 2021), which can best describe the adsorption on heterogeneous surfaces. The Freundlich isotherm equation is shown in linear form as follows:

$$\log q_e = \log K_F + \frac{1}{n} \log C_e \quad (8)$$

The  $K_F$  ( $\text{L}\cdot\text{g}^{-1}$ ) is a Freundlich constant and  $n$  is a Freundlich index. These parameters are determined by  $\log q_e$  and  $\log C_e$  (Arabpour et al., 2021).

Temkin isotherm was initially used to describe the process of gas adsorption on solid, usually used for chemical adsorption (Nezhadali et al., 2021). The isotherm model ignores the maximum or minimum concentrations of adsorbates, assuming that the adsorption heat of all molecules is a function of temperature (Al-Ghouthi et al., 2020). The linear equation is as follows:

$$q_e = A \ln K_t + B \ln C_e \quad (9)$$

**Table 3** Linear fitting parameters of MgO-AC adsorption isotherm model.

| Adsorption isotherm model | Parameter | Temperature (K) |          |          |          |
|---------------------------|-----------|-----------------|----------|----------|----------|
|                           |           | 293             | 303      | 313      | 323      |
| Langmuir                  | $q_{exp}$ | 616.5311        | 624.9419 | 639.5519 | 657.0252 |
|                           | $q_{max}$ | 593.5500        | 605.2830 | 624.7500 | 649.9000 |
|                           | $K_L$     | 0.29654         | 0.32159  | 0.37019  | 0.41437  |
|                           | $R^2$     | 0.98982         | 0.98993  | 0.99831  | 0.98054  |
| Freundlich                | $1/n$     | 0.19810         | 0.19732  | 0.19068  | 0.19224  |
|                           | $K_F$     | 260.8095        | 267.5904 | 284.1495 | 294.6580 |
|                           | $R^2$     | 0.86489         | 0.88069  | 0.86962  | 0.89837  |
| Temkin                    | $R^2$     | 0.93718         | 0.94963  | 0.94059  | 0.96308  |

where  $K_t$  ( $L \cdot mg^{-1}$ ) is the equilibrium binding constant corresponding to the maximum binding energy, constant  $B = RT/b$  represents the adsorption heat,  $R$  is the general gas constant,  $T$  is the Kelvin temperature, and  $1/b$  represents the adsorption point of the adsorbent (Ayawei et al., 2017).  $K_t$  and  $B$  can be determined from the relationship between  $q_e$  and  $C_e$ . The fitting parameters of the isotherms are listed in Table 3.

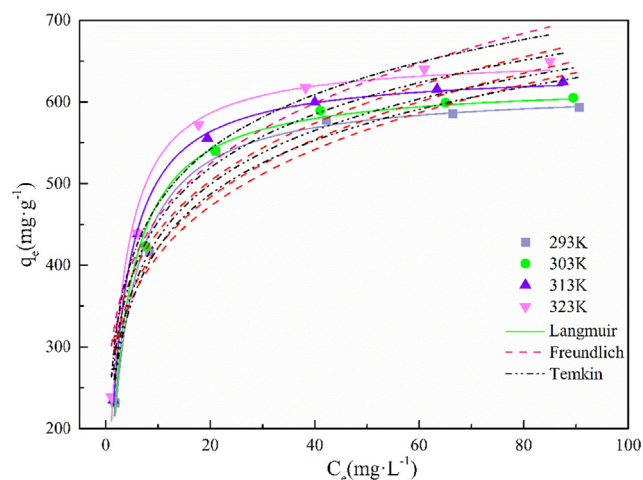
Fig. 12 shows the curve fitting graphs of three models. According to the curve fitting trend, it can be found that the amount of Cd(II) adsorbed on MgO-AC increases sharply at low concentration. With the increase of Cd(II) concentration in the solution, the adsorption capacity of MgO-AC gradually tends to the platform. According to the fitting results, compared with the other two isotherm models, the Langmuir isotherm model has better fitting degree ( $R^2 > 0.98$ ). Therefore, it is considered that the whole adsorption process is monolayer adsorption, and the process can be well represented by the Langmuir isotherm equation, indicating that the MgO-AC surface is uniform, and the adsorbate will not affect each other during the adsorption, thus inhibiting the adsorption effect (Kazeem et al., 2018). The maximum adsorption capacity calculated by Langmuir equation was  $649.90 \text{ mg} \cdot g^{-1}$ . In addition, the adsorption capacity of MgO-AC increased with the increase of temperature, indicating that the adsorption process of MgO-AC for Cd(II) was endothermic, which was consistent with the results of Khan

(Khan et al., 2020). However, it is well known that physical adsorption is usually an exothermic process, and the results of this study are opposite, which may be because the adsorption process is also accompanied by the existence of chemical adsorption. When Cd(II) is adsorbed on MgO-AC, new phases are generated, as shown in Fig. 2. The formation of chemical bonds of new phases often needs to absorb large heat to complete, and the adsorption heat generated by chemical adsorption is greater than that generated by physical adsorption, so the whole process is in an endothermic state (Xu et al., 2021a,b). In addition, the large adsorption capacity of MgO-AC materials may be attributed to the coexistence of physical adsorption and chemical adsorption.

### 3.7. Effect of microwave activation temperature and holding time on adsorption of MgO-AC

Microwave activation temperature and holding time have great influence on the pore formation of AC. Low temperature will lead to incomplete pyrolysis of materials, and some volatiles cannot fully react and volatilize. If the temperature is too high, the pores on the material surface will collapse and the specific surface area will decrease. Therefore, it is essential to explore the optimal microwave activation temperature and holding time. The pyrolysis temperature of  $Mg(NO_3)_2$  is between  $300\text{--}400 \text{ }^\circ\text{C}$ , at  $400 \text{ }^\circ\text{C}$  will be completely decomposed, taking into account the best heating temperature of AC. In this experiment, activation temperature was varied from  $500 \text{ }^\circ\text{C}$  to  $900 \text{ }^\circ\text{C}$ , and the holding time was set as follow: 20 min, 30 min, 40 min, 50 min, 60 min. For adsorption tests, 200 mL of Cd(II) solution ( $C = 100 \text{ mg} \cdot L^{-1}$ ) was mixed with 20 mg of adsorbent at different holding times and temperatures for Cd(II) removal rate determinations shown in Fig. 13.

As shown in Fig. 13, at the following conditions ( $T = 800 \text{ }^\circ\text{C}$ , holding time = 40 min, masse of MgO-AC = 20 mg and  $[Cd] = 100 \text{ mg} \cdot L^{-1}$ ), 63.7% was the highest removal rate. With the increase of heating temperature, the removal rate of Cd(II) by MgO-AC increased. This is because the amount of carbon generated by the calcination increases as the carbonization temperature increases, which will make the resulting biomass carry a larger specific surface area. Higher temperatures will also cause certain substances in biomass to volatilize, form loose porous pore structures. When the temperature reaches  $800 \text{ }^\circ\text{C}$ , the pore structure of AC is more developed. It can be seen from the diagram that when the heating temperature is rising from  $500 \text{ }^\circ\text{C}$  to  $600 \text{ }^\circ\text{C}$ , the removal rate is low, because the pyrolysis of *C. oleifera* shells chip is not

**Fig. 12** Nonlinear fitting of three isothermal models.

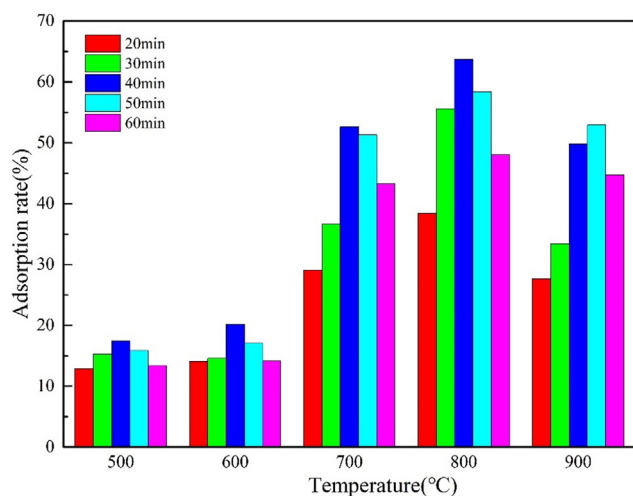


**Fig. 13** Effect of different heating conditions on Cd (II) removal by MgO-AC.

complete, and it does not provide enough adhesion sites for MgO particles, resulting in a decrease in adsorption efficiency. It can be observed from the Fig. 13 that the adsorption rate of materials at the same heating temperature increases with the increase of holding time, and the removal rate of Cd(II) reaches the maximum when the holding temperature is 40 min. This is caused by two factors: One is that the material needs sufficient time to complete pyrolysis, and the other is that the pyrolysis of  $Mg(NO_3)_2$  needs a certain time to decompose into MgO. And too long holding time will affect the specific surface area of AC, resulting in pore collapse, specific surface area decreased. In summary, microwave activation temperature of 800 °C, holding time of 40 min, can make the material completely pyrolysis and produce more complete and regular pore structure.

### 3.8. Effect of MgO addition on adsorption of MgO-AC

The addition amount of MgO is crucial for the adsorption of Cd (II). When the content of MgO is too low, the binding sites of adsorbent and heavy metal ions are less, and the adsorption capacity is low. If the MgO content is too high, the MgO molecules will flocculate with each other. MgO particles cannot be evenly distributed on the surface of AC. Large particles of MgO will have a negative impact on adsorption. The decrease of binding point will block the gap of AC and lead to the decrease of adsorption capacity. In order to make small particles of MgO evenly distributed on the surface of AC, it is necessary to add an appropriate amount of MgO content, so it is very important to explore the appropriate proportion of MgO and AC. Studies have shown that when  $\text{masse}(MgO):\text{masse}(AC) > 1:4$ , will affect the overall adsorption properties of the material, so choose  $\text{masse}(MgO):\text{masse}(AC)$  within 1/(4–20) (Tan et al., 2016; Fronczak et al., 2019; Yanagisawa et al., 2010; Benguella and Benaissa, 2002; Ahn et al., 2009; Al-Saadi et al., 2013). Using 20 mg MgO-AC adsorption 200 mL, 100  $\text{mg}\cdot\text{L}^{-1}\text{Cd}(\text{NO}_3)_2$  solution. The results are shown in Fig. 14. MgO-AC (1/4) indicates that the addition amount of MgO is 1/4 of AC. When the MgO content is 1/20 of AC content, the removal effect of Cd(II) is the best. When the MgO content is

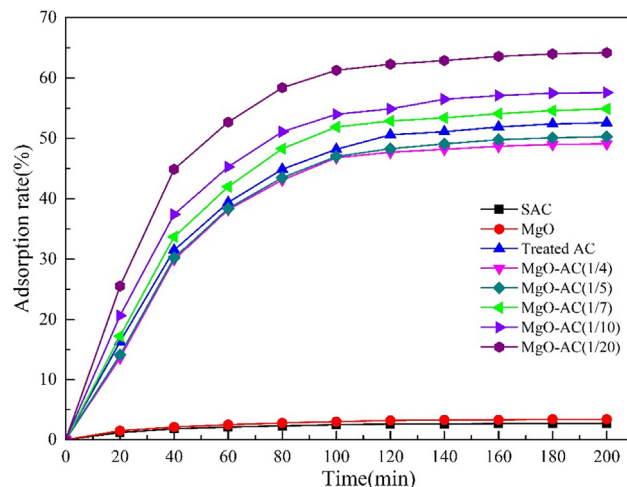


**Fig. 14** Effect of different MgO additions on Cd (II) removal by MgO-AC.

higher than 1/20, the adsorption efficiency decreases and finally tends to be stabilizes. Therefore, it can be determined that adding 1/20 times of AC mass MgO for doping modification has the best adsorption effect. In addition, compared with MgO-AC, the removal rates of SAC and MgO were only 3% when the concentration of Cd(II) was 100  $\text{mg}\cdot\text{L}^{-1}$ , and the removal rate of treated AC for Cd(II) was also lower than that of MgO-AC (1/20). It shows that the adsorption efficiency of MgO-AC on Cd(II) has played a better effect. The reason why the activity of MgO-modified AC improves the adsorption performance is that AC provides a larger adsorption carrier for MgO. At the same time, MgO-modified AC also makes AC produce more active sites, which enhances the adsorption of the two. When the AC with large specific surface area is doped with MgO, it can make MgO uniformly distribute on the AC gap and surface, avoiding agglomeration. In addition, during the adsorption process, MgO, functional groups and Cd(II) produced during biomass roasting will react to produce new substances and promote the removal of Cd(II). SAC has a large specific surface area, but due to its surface impurities, available pores are small. Treated AC has rich pores, but compared with MgO-AC, the active sites are less and the adsorption capacity is small, resulting in poor adsorption effect. In addition, the adsorption capacity of treated AC after 5 cycles is weaker than that of MgO-AC after 10 cycles, which indicates that MgO-AC has more expected adsorption capacity.

### 3.9. Kinetics study

The pseudo-second-order and the intraparticle diffusion models are used to analyze the dynamic mechanism followed by the whole adsorption process. The pseudo-second-order model is as follow (Xu et al., 2021a,b):

$$\frac{t}{q_t} = \frac{1}{k_2 q_e^2} + \frac{1}{q_e} t \quad (10)$$

The intraparticle diffusion model is as follow (Ghaemi et al., 2022):

$$q_t = k_{id} t^{0.5} \quad (11)$$

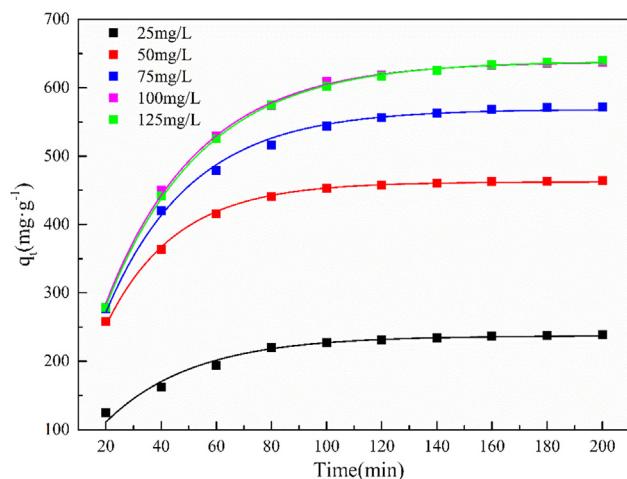


Fig. 15 Nonlinear fitting of pseudo-second-order model.

where  $q_t$  ( $\text{mg}\cdot\text{g}^{-1}$ ) represents the adsorption amount of MgO-AC in cadmium nitrate solution at time  $t$ .  $q_e$  ( $\text{mg}\cdot\text{g}^{-1}$ ) represents the adsorption amount after reaching the adsorption equilibrium.  $K_2$  and  $K_{id}$  ( $d = 1$  or  $2$ ) are two kinetic constants, which can be obtained from the slope and intercept in the fitted linear equation (Mahjoubi et al., 2017; Nyangi et al., 2021).

The adsorption process of Cd(II) on MgO-AC changes with time, as shown in Fig. 15. It can be seen that the adsorption curve had a rapid growth period in the early stage, then slowly increased, and finally reached a stable period of about 100 min.

Compared with some adsorbents in previous studies, MgO-AC had higher adsorption capacity for Cd(II) within 100 min, reaching  $602.1 \text{ mg}\cdot\text{g}^{-1}$ . In the whole adsorption process, the rapid adsorption stage is due to the high concentration of Cd(II) in the solution, which is easy to diffuse to the surface of the adsorbent and the availability of more active sites be absorbed. With the decrease of solution concentration, the negative functional groups and pores of the adsorbent are occupied by Cd(II), and the surface of the adsorbent is positively charged. The electrostatic repulsion increases, and the position of the adsorption point decreases, resulting in the decrease of the adsorption amount and the adsorption rate. In addition, the results were consistent with the results of the adsorption isotherm, indicating that the MgO-AC could effectively improve the removal effect of Cd(II). Table 4 shows the linear fitting parameters and correlation coefficients of the two equations.  $R^2$  is used to determine the fitting degree of the adsorption process and the model. From the presented results, the pseudo-second-order dynamic model has the best fitting degree with the experimental data (Ghaemi et al., 2022). The error between  $q_{e,\text{exp}}$  and  $q_{e,\text{cal}}$  is small, so the pseudo-second-order model can be used to explain the adsorption mechanism of MgO-AC for Cd(II). Fig. 16 shows the linear fitting diagrams of the two dynamic models. With the increase of the initial concentration of cadmium nitrate, the values of  $K_2$  in the pseudo-second-order model gradually decreased, indicating that the active sites on the MgO-AC surface were gradually occupied in large quantities with the increase of the initial concentration, which reduced the active sites. In addition, it

Table 4 Kinetic parameters of adsorption.

| $C_0$<br>(mg/L) | Pseudo-second-order model |                    |         |         | Intraparticle diffusion model |           |         |           |
|-----------------|---------------------------|--------------------|---------|---------|-------------------------------|-----------|---------|-----------|
|                 | $q_{e,\text{exp}}$        | $q_{e,\text{cal}}$ | $K_2$   | $R^2$   | $R_1^2$                       | $K_{i,1}$ | $R_2^2$ | $K_{i,2}$ |
| 25              | 238.7                     | 237.1              | 0.00372 | 0.99761 | 0.98118                       | 19.28348  | 0.94527 | 2.33186   |
| 50              | 464.4                     | 462.2              | 0.00198 | 0.99802 | 0.90948                       | 35.15843  | 0.92408 | 2.10495   |
| 75              | 572.1                     | 568.7              | 0.00155 | 0.99787 | 0.92783                       | 47.32411  | 0.92669 | 4.92498   |
| 100             | 637.5                     | 638.1              | 0.00137 | 0.99557 | 0.93532                       | 58.87581  | 0.94346 | 5.94785   |
| 125             | 640.3                     | 639.3              | 0.00136 | 0.99641 | 0.94018                       | 58.51305  | 0.95127 | 7.50154   |

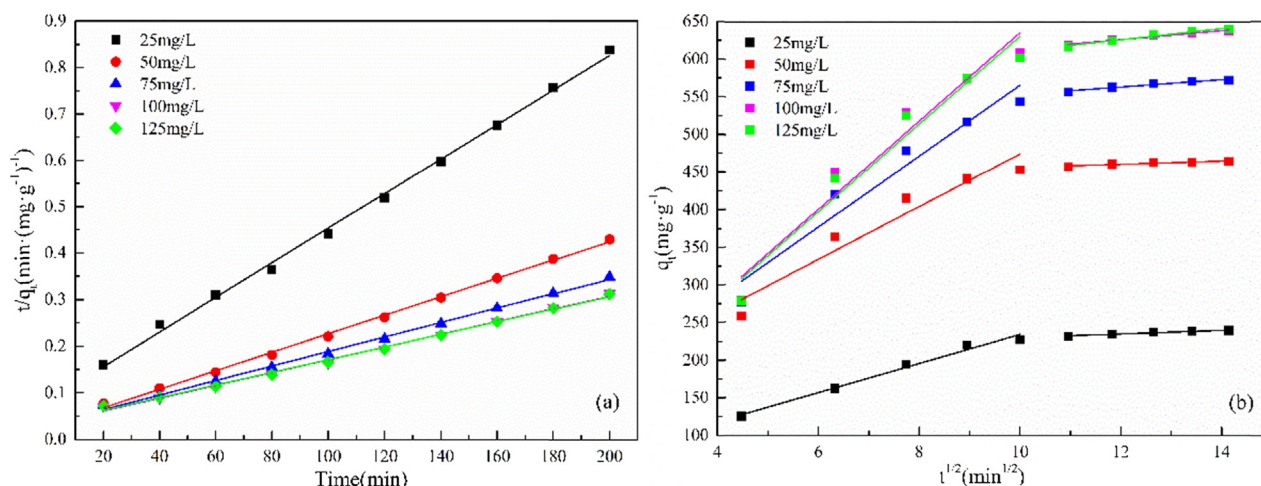
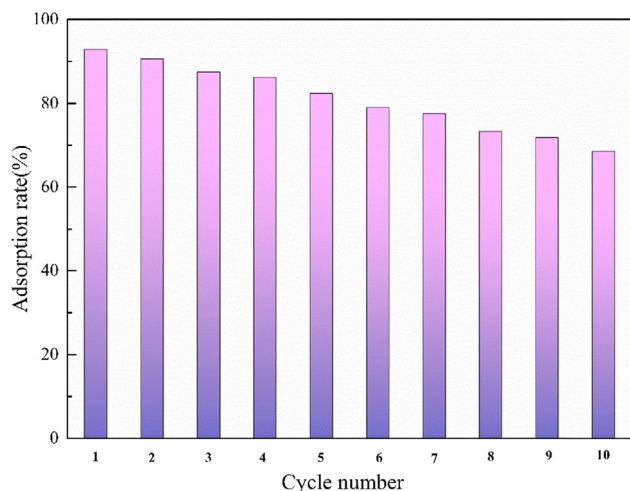


Fig. 16 Pseudo-second-order model linear fitting (a); intraparticle diffusion model linear fitting (b).



**Fig. 17** Removal efficiency of Cd(II) after ten adsorption, regeneration, and reuse.

was found that the adsorption of Cd(II) by MgO-AC could be divided into two stages by analyzing the adsorption process through the ion diffusion model, as shown in Fig. 16(b). In the initial stage, the diffusion rate constant is the largest, and then the diffusion rate decreases until the adsorption reaches a dynamic equilibrium, which is consistent with the results obtained in Fig. 15 (Tangarfa and Semaili Aouragh Hassan, 2022). In the rapid adsorption stage, the active sites on the surface of the adsorbent were largely occupied. With the adsorption process, the time transition to the second stage, the adsorption rate decreased rapidly, and the adsorption process tends to be more balanced (Hasan et al., 2021). This may be due to: (1) The adsorbent surface-active sites decreased, resulting in decreased adsorption capacity; (2) Cd(II) enter the adsorbent. With the increase of Cd(II) adsorbed in the pores, the diffusion resistance of micropores increases, resulting in the decrease of adsorption capacity (Yan et al., 2020).

### 3.10. Recycling of MgO-AC

Whether the adsorbent can be used in industrial production, in addition to considering the feasibility of its adsorption efficiency, also need to consider its economic benefits. So the renewable adsorbent is one of the necessary conditions for industrialization. The MgO-AC adsorbed Cd(II) is desorbed, and then washed and dried with deionized water for many times to achieve the purpose of MgO-AC regeneration. The

dried MgO-AC adsorbent was placed in 200 mL Cd(NO<sub>3</sub>)<sub>2</sub> solution at a concentration of 50 mg·L<sup>-1</sup>, and the operation was repeated for 10 times. Fig. 17 shows the adsorption results of cadmium nitrate by cyclic adsorption for 10 times. After two cycles of adsorption, the removal rate of Cd(NO<sub>3</sub>)<sub>2</sub> is reduced to 90.57%, and after the third cycle of adsorption, the adsorption rate is only reduced by about 5%. After cyclic adsorption for 5 times, the removal rate of Cd(II) drops to 82.34%, and the adsorption experiment is repeated. The adsorption performance of MgO-AC decreases compared with the previous five adsorption results, because the pore of AC is blocked by repeated use, resulting in the decrease of adsorption capacity. Until the experiment is repeated for 10 times, the adsorption rate of MgO-AC is reduced to 68.49%. However, this indicates that the adsorption material still has a large adsorption capacity after repeated use, which is very economical and effective for industrial wastewater treatment.

### 3.11. Comparison of adsorption capacity between MgO-AC and other adsorbents for Cd(II)

As shown in Table 5, the adsorption capacities of the MgO-AC adsorption materials in this study were compared with those of the composite materials reported previously. The results showed that under the optimal adsorption conditions, the adsorption capacity of MgO-AC was significantly better than that of the adsorbent reported in the literature, which was attributed to the fact that the production process of this work had the effect of multiple activations, which could greatly improve the number of active groups on the surface of the adsorbent, and thus showed the efficient adsorption performance for Cd(II) in water. Therefore, MgO-AC can be considered to have broad application potential in wastewater treatment.

## 4. Conclusion

MgO-AC adsorption material has been successfully prepared by microwave roasting of camellia shell soaked with magnesium nitrate and used to simulate the adsorption of Cd(II) in wastewater. The adsorption results show that MgO-AC has the characteristics of large capacity, high adsorption rate and renewable. Through XRD, XPS and FT-IR characterization, it was found that new insoluble substances were produced in the adsorption process, and they were determined to be Cd and Mg complexes. Thermodynamic data show that the adsorption process is a spontaneous endothermic process, mainly due to chemical adsorption accompanied by physical adsorption. Langmuir isotherm model and pseudo-second-order kinetic model have the best fitting degree, which can be used to describe the

**Table 5** Comparison of maximum adsorption capacity for Cd (II).

| Adsorbent                | Dose(g) | Volume (mL) | Adsorption capacity, q <sub>m</sub> (mg·g <sup>-1</sup> ) | Reference               |
|--------------------------|---------|-------------|---|-------------------------|
| DMTD-SiO <sub>2</sub>    | 0.01    | 20          | 167.33  | Hasan et al., 2021      |
| SPAC                     | 0.1     | 50          | 142.86  | Tajar et al., 2009      |
| Milled ESM-free eggshell | 0.025   | 25          | 490.19  | Baláz et al., 2015      |
| TPDP-SiO <sub>2</sub>    | 0.01    | 30          | 148.32  | Awual et al., 2018      |
| D152 resin               | 0.16    | 30          | 409   | Xiong and Yao, 2009     |
| Meranti wood             | 0.5     | 50          | 175.43  | Rafatullah et al., 2012 |
| MgO-AC                   | 0.02    | 200         | 649.9   | This work               |

adsorption mechanism. At 323 K, the maximum adsorption capacity of MgO-AC for Cd(II) is 649.9 mg·g<sup>-1</sup>. In addition, MgO-AC was mixed with Cd(II) for adsorption, regeneration and reuse, which still had high adsorption capacity after 10 times, indicating that MgO-AC was effective and feasible for the removal of heavy metals in industrial wastewater.

### CRediT authorship contribution statement

**Yingjie Xu:** Conceptualization, Data curation, Formal analysis, Investigation, Methodology, Writing – original draft. **Hongying Xia:** Conceptualization, Funding acquisition, Resources, Software, Supervision, Validation, Methodology. **Qi Zhang:** Data curation, Methodology, Writing – original draft. **Guiyu Jiang:** Data curation, Methodology, Writing – original draft. **Wuchen Cai:** Methodology. **Wenhui Hu:** Methodology.

### Declaration of Competing Interest

The authors declare that they have no known competing financial interests or personal relationships that could have appeared to influence the work reported in this paper.

### Acknowledgements

Thank Professor Xia for his financial support, guidance on experimental research and proofreading of manuscripts; thanks Dr. Zhang for the improvement of the experimental scheme and the revision of the text; thank Ms. Jiang, Mr. Cai and Mr. Hu for their suggestions and other help in the experiment. Thank the above people for their hard work in this study.

### Funding

This work was supported by the Specialized Research Fund for the National Natural Science Foundation of China (21966019), Yunan Ten Thousand Talents Plan Industrial Technology Talents Project (2019-1096), Yunan Ten Thousand Talents Plan Young & Elite Talents Project (2018-73).

### References

- Ahmadi, F., Esmaeili, H., 2018. Chemically modified bentonite/Fe<sub>3</sub>O<sub>4</sub> nanocomposite for Pb (II), Cd (II), and Ni (II) removal from synthetic wastewater. *Desalin. Water Treat.* 110, 154–167. <https://doi.org/10.5004/dwt.2018.22228>. 10.5004/dwt.2018.22228.
- Ahn, C.K., Kim, Y.M., Woo, S.H., et al, 2009. Removal of cadmium using acid-treated activated carbon in the presence of nonionic and/or anionic surfactants. *Hydrometallurgy* 99 (3–4), 209–213. <https://doi.org/10.1016/j.hydromet.2009.08.008>.
- Akinci, G., Guven, D.E., Ugurlu, S.K., 2013. Assessing pollution in Izmir Bay from rivers in western Turkey: heavy metals. *Environ. Sci. Processes Impacts* 15 (12), 2252–2262. <https://doi.org/10.1039/C3EM00333G>.
- Al-Ghouti, M.A., Da'ana, D.A., 2020a. Guidelines for the use and interpretation of adsorption isotherm models: A review. *J. Hazard. Mater.* 393, <https://doi.org/10.1016/j.jhazmat.2020.122383> 122383.
- Al-Ghouti, M.A., Razavi, M.M., 2020b. Water reuse: Brackish water desalination using *Prosopis juliflora*. *Environ. Technol. Innov.* 17, <https://doi.org/10.1016/j.eti.2020.100614> 100614.
- Alqadami, A.A., Naushad, M., Abdalla, M.A., et al, 2017. Efficient removal of toxic metal ions from wastewater using a recyclable nanocomposite: a study of adsorption parameters and interaction mechanism. *J. Cleaner Prod.* 156, 426–436. <https://doi.org/10.1016/j.jclepro.2017.04.085>.
- Al-Saadi, T.A., Saleh, A., Gupta, V.K., 2013. Spectroscopic and computational evaluation of cadmium adsorption using activated carbon produced from rubber tires. *J. Mol. Liq.* 18 (8), 136–142. <https://doi.org/10.1016/j.molliq.2013.09.036>.
- Anggraini, S.A., Uehara, M., Yamada, H., et al, 2019. Mg and Ti codoping effect on the piezoelectric response of aluminum nitride thin films. *Scr. Mater.* 159, 9–12. <https://doi.org/10.1016/j.scriptamat.2018.09.001>.
- Arabpour, A., Dan, S., Hashemipour, H., 2021. Preparation and optimization of novel graphene oxide and adsorption isotherm study of methylene blue. *Arabian J. Chem.* 14, (3). <https://doi.org/10.1016/j.arabj.2021.103003> 103003.
- Asere, T.G., Stevens, C.V., Du Laing, G., 2019. Use of (modified) natural adsorbents for arsenic remediation: a review. *Sci. Total Environ.* 676, 706–720. <https://doi.org/10.1016/j.scitotenv.2019.04.237>.
- Aslani, C.K., Amik, O., 2021. Active Carbon/PAN composite adsorbent for uranium removal: modeling adsorption isotherm data, thermodynamic and kinetic studies. *Appl. Radiat. Isot.* 168, <https://doi.org/10.1016/j.apradiso.2020.109474> 109474.
- Awual, M.R., Khraisheh, M., Alharthi, N.H., et al, 2018. Efficient detection and adsorption of cadmium (II) ions using innovative nano-composite materials. *Chem. Eng. J.* 343, 118–127. <https://doi.org/10.1016/j.cej.2018.02.116>.
- Ayawei, N., Ebelegi, A.N., Wankasi, D., 2017. Modelling and interpretation of adsorption isotherms. *J. Chem.*, 1–11 <https://doi.org/10.1155/2017/3039817>.
- Ayiania, M., Smith, M., Hensley, A.J.R., et al, 2020. Deconvoluting the XPS spectra for nitrogen-doped chars: An analysis from first principles. *Carbon* 162, 528–544. <https://doi.org/10.1016/j.carbon.2020.02.065>.
- Baláz, M., Bujňáková, Z., Baláz, P., et al, 2015. Adsorption of cadmium (II) on waste biomaterial. *J. Colloid Interface Sci.* 454, 121–133. <https://doi.org/10.1016/j.jcis.2015.03.046>.
- Belova, T.P., 2019. Adsorption of heavy metal ions (Cu<sup>2+</sup>, Ni<sup>2+</sup>, Co<sup>2+</sup> and Fe<sup>2+</sup>) from aqueous solutions by natural zeolite. *Heliyon* 5, (9). <https://doi.org/10.1016/j.heliyon.2019.e02320> e02320.
- Benguella, B., Benaissa, H., 2002. Cadmium removal from aqueous solutions by chitin: kinetic and equilibrium studies. *Water Res.* 36 (10), 2463–2474. [https://doi.org/10.1016/S0043-1354\(01\)00459-6](https://doi.org/10.1016/S0043-1354(01)00459-6).
- Borghain, X., Boruah, A., Sarma, G.K., et al, 2020. Rapid and extremely high adsorption performance of porous MgO nanostructures for fluoride removal from water. *J. Mol. Liq.* 305, <https://doi.org/10.1016/j.molliq.2020.112799> 112799.
- Botelho Junior, A.B., Vicente, A.D.A., Espinosa, D.C.R., et al, 2020. Effect of iron oxidation state for copper recovery from nickel laterite leach solution using chelating resin. *Sep. Sci. Technol.* 55 (4), 788–798. <https://doi.org/10.1080/01496395.2019.1574828>.
- Burakov, A.E., Galunin, E.V., Burakova, I.V., et al, 2018. Adsorption of heavy metals on conventional and nanostructured materials for wastewater treatment purposes: A review. *Ecotoxicol. Environ. Saf.* 148, 702–712. <https://doi.org/10.1016/j.ecoenv.2017.11.034>.
- Caballero-Briones, F., Calzadilla, O., Chale-Lara, F., et al, 2015. Mg-Doped CdS films prepared by chemical bath deposition. *Opt. Electr. Propert. Chalcogenide Lett.* 12 (4), 137–145.
- Chen, S., Wu, N.Z., Wang, P., 2004. Surface structure of benzoic acid on nano-TiO<sub>2</sub> studied by XPS. *Journal of Beijing University of Chem. Technol.* 31 (3), 48 <https://journal.buct.edu.cn/EN/Y2004/V31/I3/48>.
- Cheng, S., Chen, Q., Xia, H., et al, 2018. Microwave one-pot production of ZnO/Fe<sub>3</sub>O<sub>4</sub>/activated carbon composite for organic

- dye removal and the pyrolysis exhaust recycle. *J. Cleaner Prod.* 188, 900–910. <https://doi.org/10.1016/j.jclepro.2018.03.308>.
- Dakroury, G.A., Abo-Zahra, S.F., Hassan, H.S., 2020. Utilization of olive pomace in nano MgO modification for sorption of Ni (II) and Cu (II) metal ions from aqueous solutions. *Arabian J. Chem.* 13 (8), 6510–6522. <https://doi.org/10.1016/j.arabjc.2020.06.008>.
- Da'na, E., 2017. Adsorption of heavy metals on functionalized-mesoporous silica: A review. *Micropor. Mesopor. Mater.* 247, 145–157. <https://doi.org/10.1016/j.micromeso.2017.03.050>.
- Ding, J., Yu, C., Lu, J., et al, 2020. Enhanced CO<sub>2</sub> adsorption of MgO with alkali metal nitrates and carbonates. *Appl. Energy* 263, <https://doi.org/10.1016/j.apenergy.2020.114681>.
- Duan, G., Cao, Z., Zhong, H., et al, 2022. Highly efficient poly (6-acryloylamino-N-hydroxyhexanamide) resin for adsorption of heavy metal ions. *J. Environ. Manage.* 308, <https://doi.org/10.1016/j.jenvman.2022.114631>.
- Duan, C., Ma, T., Wang, J., et al, 2020. Removal of heavy metals from aqueous solution using carbon-based adsorbents: A review. *J. Water Process Eng.* 37, <https://doi.org/10.1016/j.jwpe.2020.101339>.
- Elashry, S.M., Labib, S., Attallah, M.F., 2022. Sorption behavior of natural uranium from aqueous solutions using modified activated carbon with quinoline. *Radiochim. Acta* 110 (3), 157–171. <https://doi.org/10.1515/ract-2021-1071>.
- Esmaili, H., Mousavi, S.M., Hashemi, S.A., et al, 2021. Activated carbon@ MgO@ Fe<sub>3</sub>O<sub>4</sub> as an efficient adsorbent for As (III) removal. *Carbon Lett.* 31 (5), 851–862. <https://doi.org/10.1007/s42823-020-00186-2>.
- Feng, P., Li, J., Wang, H., et al, 2020. Biomass-based activated carbon and activators: preparation of activated carbon from corncob by chemical activation with biomass pyrolysis liquids. *ACS Omega* 5 (37), 24064–24072. <https://doi.org/10.1021/acsomega.0c03494>.
- Foroutan, R., Mohammadi, R., Ahmadi, A., et al, 2022. Impact of ZnO and Fe<sub>3</sub>O<sub>4</sub> magnetic nanoscale on the methyl violet 2B removal efficiency of the activated carbon oak wood. *Chemosphere* 286, <https://doi.org/10.1016/j.chemosphere.2021.131632>.
- Fronczak, M., Pyrzyńska, K., Bhattarai, A., et al, 2019. Improved adsorption performance of activated carbon covalently functionalised with sulphur-containing ligands in the removal of cadmium from aqueous solutions. *Int. J. Environ. Sci. Technol.* 16 (12), 7921–7932. <https://doi.org/10.1007/s13762-019-02398-0>.
- Fu, C., Zhu, X., Dong, X., et al, 2021. Study of adsorption property and mechanism of lead (II) and cadmium (II) onto sulfhydryl modified attapulgite. *Arabian J. Chem.* 14, (2). <https://doi.org/10.1016/j.arabjc.2020.102960>.
- Gao, M., Wang, Z., Yang, C., et al, 2019. Novel magnetic graphene oxide decorated with persimmon tannins for efficient adsorption of malachite green from aqueous solutions. *Colloids Surf., A* 566, 48–57. <https://doi.org/10.1016/j.colsurfa.2019.01.016>.
- Ghaemi, A., Mashhadimoslem, H., Zohourian, I.P., 2021. NiO and MgO/activated carbon as an efficient CO<sub>2</sub> adsorbent: characterization, modeling, and optimization. *Int. J. Environ. Sci. Technol.*, 727–746 <https://doi.org/10.1007/s13762-021-03582-x>.
- Ghaemi, A., Mashhadimoslem, H., Zohourian, I.P., 2022. NiO and MgO/activated carbon as an efficient CO<sub>2</sub> adsorbent: characterization, modeling, and optimization. *Int. J. Environ. Sci. Technol.* 19 (2), 727–746. <https://doi.org/10.1007/s13762-021-03582-x>.
- Ghalekhondabi, V., Fazlali, A., Ketabi, K., 2021. Synthesis and characterization of modified activated carbon (MgO/AC) for methylene blue adsorption: optimization, equilibrium isotherm and kinetic studies. *Water Sci. Technol.* 83 (7), 1548–1565. <https://doi.org/10.2166/wst.2021.016>.
- Gokce, Y., Aktas, Z., 2014. Nitric acid modification of activated carbon produced from waste tea and adsorption of methylene blue and phenol. *Appl. Surf. Sci.* 313, 352–359. <https://doi.org/10.1016/j.apsusc.2014.05.214>.
- Goswami, M., Phukan, P., 2017. Enhanced adsorption of cationic dyes using sulfonic acid modified activated carbon. *J. Environ. Chem. Eng.* 5 (4), 3508–3517. <https://doi.org/10.1016/j.jece.2017.07.016>.
- Guo, F., Jiang, X., Li, X., et al, 2020. Synthesis of MgO/Fe<sub>3</sub>O<sub>4</sub> nanoparticles embedded activated carbon from biomass for high-efficient adsorption of malachite green. *Mater. Chem. Phys.* 240, <https://doi.org/10.1016/j.matchemphys.2019.122240>.
- Guo, J., Song, Y., Ji, X., et al, 2019. Preparation and characterization of nanoporous activated carbon derived from prawn shell and its application for removal of heavy metal ions. *Materials* 12 (2), 241. <https://doi.org/10.3390/ma12020241>.
- Gupta, A.D., Rawat, K.P., Bhadauria, V., et al, 2021. Recent trends in the application of modified starch in the adsorption of heavy metals from water: a review. *Carbohydr. Polym.* 269, <https://doi.org/10.1016/j.carbpol.2021.117763>.
- Haidari, S., Kamarehie, B., Jafari, A., et al, 2016. Oxalic acid degradation from aqueous solution using ozonation process in the presence of magnesium oxide nanoparticles catalyst stabilized on activated carbon. *Int. J. Environ. Health Eng.* 5 (1), 23. <https://doi.org/10.4103/2277-9183.196665>.
- Hakim, A., Tahari, M.N.A., Marliza, T.S., et al, 2015. Study of CO<sub>2</sub> adsorption and desorption on activated carbon supported iron oxide by temperature programmed desorption. *Jurnal Teknologi* 77 (33), 75–84. <https://doi.org/10.11113/jt.v77.7010>.
- Hasan, M.N., Salman, M.S., Islam, A., et al, 2021. Sustainable composite sensor material for optical cadmium (II) monitoring and capturing from wastewater. *Microchem. J.* 161, <https://doi.org/10.1016/j.microc.2020.105800>.
- Hashem, A., Aniagor, C.O., Nasr, M.F., et al, 2021. Efficacy of treated sodium alginate and activated carbon fibre for Pb (II) adsorption. *Int. J. Biol. Macromol.* 176, 201–216. <https://doi.org/10.1016/j.ijbiomac.2021.02.067>.
- Hua, Q.X., Tang, J.W., Liu, Y., et al, 2010. Adsorption of phosphate in waste water with steel slag. *Chin. J. Process Eng.* 10 (1), 75–78. <https://doi.org/10.1007/s10075-010-0075-05>.
- Igwegbe, C.A., Ighalo, J.O., Onyechi, K.K., et al, 2021. Adsorption of Congo red and malachite green using H<sub>3</sub>PO<sub>4</sub> and NaCl-modified activated carbon from rubber (*Hevea brasiliensis*) seed shells. *Sustain. Water Resour. Manage.* 7 (4), 1–16. <https://doi.org/10.1007/s40899-021-00544-6>.
- Jian, X., Zhuang, X., Li, B., et al, 2018. Comparison of characterization and adsorption of biochars produced from hydrothermal carbonization and pyrolysis. *Environ. Technol. Innovation* 10, 27–35. <https://doi.org/10.1016/j.eti.2018.01.004>.
- Jun, B.M., Kim, S., Kim, Y., et al, 2019. Comprehensive evaluation on removal of lead by graphene oxide and metal organic framework. *Chemosphere* 231, 82–92. <https://doi.org/10.1016/j.chemosphere.2019.05.076>.
- Kazeem, T.S., Lateef, S.A., Ganiyu, S.A., et al, 2018. Aluminium-modified activated carbon as efficient adsorbent for cleaning of cationic dye in wastewater. *J. Cleaner Prod.* 205, 303–312. <https://doi.org/10.1016/j.jclepro.2018.09.114>.
- Khajuria, P., Mahajan, R., Kumar, S., et al, 2020. Surface and spectral investigation of Sm<sup>3+</sup> doped MgO-ZrO<sub>2</sub> phosphor. *Optik* 216, <https://doi.org/10.1016/j.ijleo.2020.164909>.
- Khan, Z.H., Gao, M., Qiu, W., et al, 2020. Mechanisms for cadmium adsorption by magnetic biochar composites in an aqueous solution. *Chemosphere* 246, <https://doi.org/10.1016/j.chemosphere.2019.125701>.
- Khan, A., Naeem, A., Mahmood, T., et al, 2022. Mechanistic study on methyl orange and congo red adsorption onto polyvinyl pyrrolidone modified magnesium oxide. *Int. J. Environ. Sci. Technol.* 19 (4), 2515–2528. <https://doi.org/10.1007/s13762-021-03308-z>.
- Kumar, J.A., Amarnath, D.J., Jabasingh, S.A., et al, 2019. One pot Green Synthesis of Nano magnesium oxide-carbon composite: Preparation, characterization and application towards anthracene

- adsorption. *J. Cleaner Prod.* 237,. <https://doi.org/10.1016/j.jclepro.2019.117691> 117691.
- Li, H., Dong, X., da Silva, E.B., et al, 2017. Mechanisms of metal sorption by biochars: biochar characteristics and modifications. *Chemosphere* 178, 466–478. <https://doi.org/10.1016/j.chemosphere.2017.03.072>.
- Li, L., Hu, W., Gao, Z., et al, 2016. Kinematics analysis and experiment of crank rocker vibrating coarse sorting machine for unshelled oil-tea fruit. *Transactions of the Chinese Society of Agric. Eng.* 32 (7), 28–35. <https://doi.org/10.11975/j.issn.1002-6819.2016.07.004>.
- Li, J., Wang, X., Zhao, G., et al, 2018. Metal–organic framework-based materials: superior adsorbents for the capture of toxic and radioactive metal ions. *Chem. Soc. Rev.* 47 (7), 2322–2356. <https://doi.org/10.1039/C7CS00543A>.
- Lima, E.C., Hosseini-Bandegharai, A., Moreno-Piraján, J.C., et al, 2019. A critical review of the estimation of the thermodynamic parameters on adsorption equilibria. Wrong use of equilibrium constant in the Van't Hoff equation for calculation of thermodynamic parameters of adsorption. *J. Mol. Liq.* 273, 425–434. <https://doi.org/10.1016/j.molliq.2018.10.048>.
- Liu, X., He, C., Yu, X., et al, 2018. Net-like porous activated carbon materials from shrimp shell by solution-processed carbonization and H<sub>3</sub>PO<sub>4</sub> activation for methylene blue adsorption. *Powder Technol.* 326, 181–189. <https://doi.org/10.1016/j.powtec.2017.12.034>.
- Liu, T., Lawluy, Y., Shi, Y., et al, 2022. Adsorption of cadmium and lead from aqueous solution using modified biochar: a review. *J. Environ. Chem. Eng.* 10, (1). <https://doi.org/10.1016/j.jece.2021.106502> 106502.
- Liu, Q., Li, Y., Chen, H., et al, 2020. Superior adsorption capacity of functionalised straw adsorbent for dyes and heavy-metal ions. *J. Hazard. Mater.* 382,. <https://doi.org/10.1016/j.jhazmat.2019.121040> 121040.
- Luo, S., Xu, X., Zhou, G., et al, 2014. Amino siloxane oligomer-linked graphene oxide as an efficient adsorbent for removal of Pb (II) from wastewater. *J. Hazard. Mater.* 274, 145–155. <https://doi.org/10.1016/j.jhazmat.2014.03.062>.
- Mahjoubi, F.Z., Khalidi, A., Cherkaoui, O., et al, 2017. Treatment of textile effluents by chloride-intercalated Zn-, Mg-and Ni-Al layered double hydroxides. *Journal of Water Reuse and Desalination* 7 (3), 307–318. <https://doi.org/10.2166/wrd.2016.041>.
- Miao, Q., Li, G., 2021. Potassium phosphate/magnesium oxide modified biochars: Interfacial chemical behaviours and Pb binding performance. *Sci. Total Environ.* 759,. <https://doi.org/10.1016/j.scitotenv.2020.143452> 143452.
- Ming, W., Yoon, M., Du, M.H., et al, 2016. First-principles prediction of thermodynamically stable two-dimensional electrides. *J. Am. Chem. Soc.* 138 (47), 15336–15344. <https://doi.org/10.1021/jacs.6b05586>.
- Muttakin, M., Mitra, S., Thu, K., et al, 2018. Theoretical framework to evaluate minimum desorption temperature for IUPAC classified adsorption isotherms. *Int. J. Heat Mass Transf.* 122, 795–805. <https://doi.org/10.1016/j.ijheatmasstransfer.2018.01.107>.
- Naushad, M., Vasudevan, S., Sharma, G., et al, 2016. Adsorption kinetics, isotherms, and thermodynamic studies for Hg<sup>2+</sup> adsorption from aqueous medium using alizarin red-S-loaded amberlite IRA-400 resin. *Desalin. Water Treat.* 57 (39), 18551–18559. <https://doi.org/10.1080/19443994.2015.1090914>.
- Naushad, M., Alqadami, A.A., AlOthman, Z.A., et al, 2019. Adsorption kinetics, isotherm and reusability studies for the removal of cationic dye from aqueous medium using arginine modified activated carbon. *J. Mol. Liq.* 293,. <https://doi.org/10.1016/j.molliq.2019.111442> 111442.
- Nezhadali, A., Koushali, S.E., Divsar, F., 2021. Synthesis of polypyrrole–chitosan magnetic nanocomposite for the removal of carbamazepine from wastewater: Adsorption isotherm and kinetic study. *J. Environ. Chem. Eng.* 9, (4). <https://doi.org/10.1016/j.jece.2021.105648> 105648.
- Nyangi, M.J., Chebude, Y., Kilulya, K.F., et al, 2021. Comparative study on adsorption isotherm and kinetics of defluoridation using aluminum and iron electrodes in electrocoagulation. *Chem. Afr.* 4 (2), 391–398. <https://doi.org/10.1007/s42250-021-00228-w>.
- Otunola, B.O., Ololade, O.O., 2020. A review on the application of clay minerals as heavy metal adsorbents for remediation purposes. *Environ. Technol. Innovation* 18,. <https://doi.org/10.1016/j.eti.2020.100692> 100692.
- Park, C.M., Han, J., Chu, K.H., et al, 2017. Influence of solution pH, ionic strength, and humic acid on cadmium adsorption onto activated biochar: experiment and modeling. *J. Ind. Eng. Chem.* 48, 186–193. <https://doi.org/10.1016/j.jiec.2016.12.038>.
- Przepiórski, J., Czyżewski, A., Pietrzak, R., et al, 2013. MgO/CaO-loaded activated carbon for carbon dioxide capture: practical aspects of use. *Ind. Eng. Chem. Res.* 52 (20), 6669–6677. <https://doi.org/10.1021/ie302848r>.
- Pushpa, T.B., Vijayaraghavan, J., Basha, S.J.S., et al, 2015. Investigation on removal of malachite green using EM based compost as adsorbent. *Ecotoxicol. Environ. Saf.* 118, 177–182. <https://doi.org/10.1016/j.ecoenv.2015.04.033>.
- Rafatullah, M., Sulaiman, O., Hashim, R., et al, 2012. Removal of cadmium (II) from aqueous solutions by adsorption using meranti wood. *Wood Sci. Technol.* 46 (1), 221–241. <https://doi.org/10.1007/s00226-010-0374-y>.
- Salamat, S., Hadavifar, M., Rezaei, H., 2019. Preparation of nanochitosan-STP from shrimp shell and its application in removing of malachite green from aqueous solutions. *J. Environ. Chem. Eng.* 7, (5). <https://doi.org/10.1016/j.jece.2019.103328> 103328.
- Saleh, T.A., 2016. Nanocomposite of carbon nanotubes/silica nanoparticles and their use for adsorption of Pb (II): from surface properties to sorption mechanism. *Desalin. Water Treat.* 57 (23), 10730–10744. <https://doi.org/10.1080/19443994.2015.1036784>.
- Shahrokhi-Shahraki, R., Benally, C., El-Din, M.G., et al, 2021. High efficiency removal of heavy metals using tire-derived activated carbon vs commercial activated carbon: Insights into the adsorption mechanisms. *Chemosphere* 264,. <https://doi.org/10.1016/j.chemosphere.2020.128455> 128455.
- Sing, K.S.W., 1985. Reporting physisorption data for gas/solid systems with special reference to the determination of surface area and porosity (Recommendations 1984). *Pure Appl. Chem.* 57 (4), 603–619. <https://doi.org/10.1351/pac198557040603>.
- Singh, N.B., Nagpal, G., Agrawal, S., 2018. Water purification by using adsorbents: a review. *Environ. Technol. Innov.* 11, 187–240. <https://doi.org/10.1016/j.eti.2018.05.006>.
- Soto-Ramirez, R., Lobos, M.G., Córdova, O., et al, 2021. Effect of growth conditions on cell wall composition and cadmium adsorption in *Chlorella vulgaris*: A new approach to biosorption research. *J. Hazard. Mater.* 411,. <https://doi.org/10.1016/j.jhazmat.2021.125059> 125059.
- Tajar, A.F., Kaghazchi, T., Soleimani, M., 2009. Adsorption of cadmium from aqueous solutions on sulfurized activated carbon prepared from nut shells. *J. Hazard. Mater.* 165 (1–3), 1159–1164. <https://doi.org/10.1016/j.jhazmat.2008.10.131>.
- Tan, I.A.W., Chan, J.C., Hameed, B.H., et al, 2016. Adsorption behavior of cadmium ions onto phosphoric acid-impregnated microwave-induced mesoporous activated carbon. *J. Water Process Eng.* 14, 60–70. <https://doi.org/10.1016/j.jwpe.2016.10.007>.
- Tangarfa, M., Semlali Aouragh Hassan, N., 2022. The behaviour of tannic acid adsorption on fluorite surface: Isotherm, kinetic and thermodynamic studies. *Physicochem. Problems Min. Process.* 58. <https://doi.org/10.37190/ppmp/144288>.
- Tao, H.C., Zhang, H.R., Li, J.B., et al, 2015. Biomass based activated carbon obtained from sludge and sugarcane bagasse for removing lead ion from wastewater. *Bioresour. Technol.* 192, 611–617. <https://doi.org/10.1016/j.biortech.2015.06.006>.

- Tian, H., Jiao, L., Dong, D., 2019. Rapid determination of trace cadmium in drinking water using laser-induced breakdown spectroscopy coupled with chelating resin enrichment. *Sci. Rep.* 9 (1), 1–8. <https://doi.org/10.1038/s41598-019-46924-z>.
- Verma R, Dwivedi P. Heavy metal water pollution-A case study. *Recent Research in Science and Technology*, 2013, 5(5). ISSN: 2076-5061. <https://www.researchgate.net/publication/303152384>.
- Vu, A.T., Ho, K., Lee, C.H., 2016. Removal of gaseous sulfur and phosphorus compounds by carbon-coated porous magnesium oxide composites. *Chem. Eng. J.* 283, 1234–1243. <https://doi.org/10.1016/j.cej.2015.08.083>.
- Wang, J., Chen, Z., Chen, B., 2014. Adsorption of polycyclic aromatic hydrocarbons by graphene and graphene oxide nanosheets. *Environ. Sci. Technol.* 48 (9), 4817–4825. <https://doi.org/10.1021/es405227u>.
- Wang, S., Lee, Y.R., Won, Y., et al, 2022. Development of high-performance adsorbent using KOH-impregnated rice husk-based activated carbon for indoor CO<sub>2</sub> adsorption. *Chem. Eng. J.* 437, <https://doi.org/10.1016/j.cej.2022.135378> 135378.
- Wang, G.X., Li, G., Mao, X.B., 2007. Thermodynamics study on the adsorption of cordycepin by cation-exchange resin. *J. Chongqing Univ. (Nat. Sci. Ed.)* 30 (9), 105–108. 1000-582X (2007)09-0105-04.
- Wattigney, W.A., Irvin-Barnwell, E., Li, Z., et al, 2019. Biomonitoring programs in Michigan, Minnesota and New York to assess human exposure to Great Lakes contaminants. *Int. J. Hyg. Environ. Health* 222 (1), 125–135. <https://doi.org/10.1016/j.ijheh.2018.08.012>.
- WHO, Guidelines for Drinking-water Quality, 4th ed.
- Xiong, C.H., Yao, C.P., 2009. Study on the adsorption of cadmium (II) from aqueous solution by D152 resin. *J. Hazard. Mater.* 166 (2–3), 815–820. <https://doi.org/10.1016/j.jhazmat.2008.11.082>.
- Xu, Y., Zhang, Q., Jiang, G., et al, 2021b. Activated Carbon Loaded with Ti<sup>3+</sup> Self-Doped TiO<sub>2</sub> Composite Material Prepared by Microwave Method. *J. Mater. Eng. Perform.*, 1–13 <https://doi.org/10.1007/s11665-021-06421-9>.
- Xu, H., Zhu, S., Xia, M., et al, 2021a. Rapid and efficient removal of diclofenac sodium from aqueous solution via ternary core-shell CS@ PANI@ LDH composite: experimental and adsorption mechanism study. *J. Hazard. Mater.* 402, <https://doi.org/10.1016/j.jhazmat.2020.123815> 123815.
- Xu, H., Zhu, S., Xia, M., et al, 2022. Three-dimension hierarchical composite via in-situ growth of Zn/Al layered double hydroxide plates onto polyaniline-wrapped carbon sphere for efficient naproxen removal. *J. Hazard. Mater.* 423, <https://doi.org/10.1016/j.jhazmat.2021.127192> 127192.
- Yan, Y., Chu, Y., Khan, M.A., et al, 2022. Facile immobilization of ethylenediamine tetramethylene-phosphonic acid into UiO-66 for toxic divalent heavy metal ions removal: An experimental and theoretical exploration. *Sci. Total Environ.* 806, <https://doi.org/10.1016/j.scitotenv.2021.150652> 150652.
- Yan, H., Hu, W., Cheng, S., et al, 2020. Microwave-assisted preparation of manganese dioxide modified activated carbon for adsorption of lead ions. *Water Sci. Technol.* 82 (1), 170–184. <https://doi.org/10.2166/wst.2020.350>.
- Yanagisawa, H., Matsumoto, Y., Machida, M., 2010. Adsorption of Zn (II) and Cd (II) ions onto magnesium and activated carbon composite in aqueous solution. *Appl. Surf. Sci.* 256 (6), 1619–1623. <https://doi.org/10.1016/j.apsusc.2009.10.010>.
- Yang, C., Wang, Y., Fan, H., et al, 2020. Bifunctional ZnO-MgO/activated carbon adsorbents boost H<sub>2</sub>S room temperature adsorption and catalytic oxidation. *Appl. Catal. B* 266, <https://doi.org/10.1016/j.apcatb.2020.118674> 118674.
- Yang, Z., Zhao, Z., Yang, X., et al, 2021. Xanthate modified magnetic activated carbon for efficient removal of cationic dyes and tetracycline hydrochloride from aqueous solutions. *Colloids Surf., A* 615, <https://doi.org/10.1016/j.colsurfa.2021.126273> 126273.
- Yoo, H., Lee, M.W., Lee, S., et al, 2020. Enhancing photocatalytic β-O-4 bond cleavage in lignin model compounds by silver-exchanged cadmium sulfide. *ACS Catal.* 10 (15), 8465–8475. <https://doi.org/10.1021/acscatal.0c01915>.
- Zhang, Y., Ma, M., Zhang, X., et al, 2014. Synthesis, characterization, and catalytic property of nanosized MgO flakes with different shapes. *J. Alloy. Compd.* 590, 373–379. <https://doi.org/10.1016/j.jallcom.2013.12.113>.
- Zhang, Y., Guo, X., Wu, F., et al, 2016. Mesocarbon microbead carbon-supported magnesium hydroxide nanoparticles: turning spent Li-ion battery anode into a highly efficient phosphate adsorbent for wastewater treatment. *ACS Appl. Mater. Interfaces* 8 (33), 21315–21325. <https://doi.org/10.1021/acsami.6b05458>.
- Zhou, K., Li, L., Ma, X., et al, 2018. Activated carbons modified by magnesium oxide as highly efficient sorbents for acetone. *RSC Adv.* 8 (6), 2922–2932. <https://doi.org/10.1039/C7RA11740J>.
- Zhu, S., Chen, Y., Khan, M.A., et al, 2022a. In-Depth Study of Heavy Metal Removal by an Etidronic Acid-Functionalized Layered Double Hydroxide. *ACS Appl. Mater. Interfaces* 14 (5), 7450–7463. <https://doi.org/10.1021/acsami.1c22035>.
- Zhu, S., Khan, M.A., Kameda, T., et al, 2022b. New insights into the capture performance and mechanism of hazardous metals Cr<sup>3+</sup> and Cd<sup>2+</sup> onto an effective layered double hydroxide based material. *J. Hazard. Mater.* 426, 128062. <https://doi.org/10.1016/j.jhazmat.2021.128062>.